
Article:
Fremmelev, M.A. orcid.org/0000-0003-4729-6569, Ladpli, P., Orlowitz, E. et al. (3 more authors) (2023) A full-scale wind turbine blade monitoring campaign: detection of damage initiation and progression using medium-frequency active vibrations. Structural Health Monitoring. ISSN 1475-9217

https://doi.org/10.1177/14759217231163471

Journal Title
XX(X):1–20

DOI: 10.1177/ToBeAssigned
www.sagepub.com/
SAGE

A full-scale wind turbine blade monitoring campaign: Detection of damage initiation and progression using medium-frequency active vibrations

Mads Anker Fremmelev[1,4], Purim Ladpli[1], Esben Orlowitz[2], Nikolaos Dervilis[3], Malcolm McGugan[4] and Kim Branner[4]

Abstract

This work is concerned with a structural health monitoring (SHM) campaign of a 52-meter wind turbine blade. Multiple artificial damages are introduced in the blade sequentially, and fatigue testing is conducted with each damage in sequence. Progressive fatigue-driven damage propagation is achieved, enabling investigations concerning detection of initiation and propagation of damage in the blade. Using distributed accelerometers, operational modal analysis is performed to extract the lower-order natural vibration modes of the blade, which are shown to not be sensitive to small damages in the blade. To enable monitoring of small damages, an active vibration monitoring system is used, comprised of an electrodynamic vibration shaker and distributed accelerometers. From the accelerometer data, frequency domain methods are used to extract features. Using the extracted features, outlier detection is performed to investigate changes in the measurements resulting from the introduced damages. Capabilities of using features based on the active vibration data for detection of initiation and progression of damage in a wind turbine blade during fatigue testing are investigated, showing good correlation between the observed damage progression and the calculated changes in the damage index.

Keywords

Wind turbine blades, damage, operational modal analysis, active vibration input, outlier detection

Introduction

To enable the transition to renewable energy sources, it is necessary to reduce costs and ensure availability of wind energy. Operations and maintenance (O&M) costs of offshore turbines make up 25 - 30% of the whole life cycle costs[1]. From a business perspective, blades are one of the most critical components in wind turbines, both concerning failure rates and downtime[2], and as such one of the main contributors to O&M costs. To reduce blade-related O&M costs, it is necessary to detect damages in blades at an early stage, before they significantly affect the structural integrity of blades. Repairs of small damages can be performed up-tower, which is significantly less demanding in regards to man-hours and equipment than demounting blades and performing ground-based repairs, which is necessary for more severe damages. If damages are not detected before they grow to a critical size, replacement with a new blade may be necessary. In the worst case, blade failure may occur, which can cause significant damage to the drive train and the generator, or even damage to the tower and consequently total loss of the turbine.

To ensure that damages present in wind turbine blades are detected at an early stage, the development of structural health monitoring (SHM) systems for wind turbine blades is becoming increasingly important[3]. Various sensor types, measuring different physical responses, have been researched for use in blade SHM[4,5]. One sensing modality being used for SHM is vibrations, which in practice is based on acceleration measurements. Vibration-based methods have shown great promise for SHM of various wind turbine components, such as gearboxes and towers. In recent years, vibration-based methods have received increasing attention from researchers for use in SHM of wind turbine blades. Vibration-based methods are based on the assumption that the modal parameters, e.g. eigenfrequencies and mode shapes, of structures are altered due to the occurrence of damages. The presence of damage in a structure alters the stiffness of the structure, which is reflected through changes in the modal parameters of the structure. One inherent challenge in vibration-based SHM is that smaller wavelengths, i.e. higher frequency vibrations, are necessary for detection of small damages. However, with increasing vibration frequency comes higher attenuation of the signal, which limits the detection range. As such, the challenge is to find an appropriate compromise between detectable damage size and detection range. With modern wind turbine

[1]Siemens Gamesa Renewable Energy, Blade Submodules Technology, Assensvej 11, 9220 Aalborg East, Denmark
[2]Siemens Gamesa Renewable Energy, Turbine Measurement Operation, Borupvej 16, 7330 Brande, Denmark
[3]University of Sheffield, Dynamics Research Group, Department of Mechanical Engineering, S1 3JD, Sheffield, United Kingdom
[4]Technical University of Denmark, Department of Wind and Energy Systems, Frederiksborgvej 399, 4000 Roskilde, Denmark

Corresponding author:
Mads Anker Fremmelev, Siemens Gamesa Renewable Energy Assensvej 11, Aalborg East, 9220, Denmark.
Email: mads.fremmelev@siemensgamesa.com

blades surpassing 100 meters in length, this is becoming increasingly relevant, since the number of sensors used per blade needs to be kept at a minimum to reduce costs.

Vibration-based SHM methods are based on measurement of the acceleration response of a structure, which is used as a feature for detection of changes in the structure. One such vibration-based SHM method relies on extraction of the natural vibration modes of a structure and monitoring the associated modal parameters, such as eigenfrequencies and mode shapes. One way to estimate the modal parameters of a structure is through operational modal analysis (OMA), which is an output-only method. Consequently, it is not necessary to measure the applied excitation in the form of e.g. hammer hits and ambient loading, and it is only necessary to measure the vibration response of a structure. The method relying on output-only measurements enables its practical application in structures subjected to environmental excitation, such as wind turbines.

An industrial software solution for modal-parameter-based SHM has been developed by e.g. Structural Vibration Solutions[6]. The use of different methods for extracting modal parameters of wind turbines has been studied. Acceleration- and strain-based OMA of wind turbine blades was performed, and good agreement in modal parameters of two nominally identical blades was found[7,8]. Comparison of modal parameter estimation between modal parameters extracted with experimental modal analysis using hammer and shaker excitation, respectively, yielded results with little difference[9]. OMA has been used to detect changes in the modal parameters of a 6.5-meter wind turbine blade caused by buckling-induced damage[10]. Eigenfrequencies, mode shapes, and mode shape curvatures showed detectable changes resulting from the damage. Another study using OMA for damage detection in wind turbine blades investigated changes to modal parameters in a 34-meter blade on a test stand due to the presence of a trailing edge opening[11]. Eigenfrequencies and mode shapes were not significantly affected by the introduced damage. OMA and the continuous wavelet transform were used to locate local changes in the mode shapes of the previously mentioned 34-meter blade, which yielded information on the location and size of the introduced damage[12]. Use of eigenfrequencies for detection of a 0.2 - 1.0 meter crack between the shear web and spar cap in a 45.7-meter wind turbine blade was investigated, and no significant changes in eigenfrequencies were detected as a consequence of the damage[13].

In a previous study, the authors used OMA to estimate the modal parameters of the lower-order natural vibration modes of a 52-meter wind turbine blade mounted on a test stand[14]. Neither eigenfrequencies nor mode shapes showed significant changes resulting from manually induced transverse laminate cracks of lengths up to approximately 1% of the blade length. Thus, the modal parameters from lower-order natural vibration modes are not deemed to be reliable features for timely detection of damages in wind turbine blades.

Given that the literature shows that monitoring of lower-order natural vibration modes, i.e. vibrations in the low-frequency range, is not reliable for timely detection of damages in wind turbine blades, it is necessary to use vibrations in a higher frequency range. One method relying on passive monitoring of high-frequency vibrations is through the use of acoustic emission (AE) sensors. In the laminate of wind turbine blades, matrix or fiber breakage will result in emission of high-frequency vibrations, which can be measured with AE sensors. AE sensors were used in a fatigue test to failure of a 14.3-meter blade to perform localized monitoring of different types of artificial damages[15]. Data from the AE sensors showed progressive damage development over the course of the fatigue test. From the AE data, it was also apparent at which point in time critical failure of the blade was imminent. AE sensors were used by the authors during fatigue testing of a 52-meter blade with manually induced transverse laminate cracks[14]. The AE sensors were used to conduct localized monitoring of fatigue-driven damage propagation, where a detection range of 0.5 meters was obtained for damage propagation in the shear web and spar cap laminate.

Passive monitoring of high-frequency vibrations shows great promise for localized SHM of wind turbine blades. Due to the high attenuation of high-frequency vibrations in composite laminate materials, the detection range is rather limited. Thus, a high number of sensors is necessary for monitoring of larger areas of wind turbine blades, which results in a cost-prohibitive SHM system. As an alternative solution, monitoring systems using active vibration inputs have been studied. Through active excitation of a structure at high amplitudes with a given frequency range, the frequency content of the active vibration signal can be monitored, and the influence of damage on the frequency content can be studied.

A guided waves pitch-catch system was used to monitor impact damage in a carbon fiber plate[16]. A high-frequency active vibration input was applied in the form of a sinusoidal chirp between 10 kHz - 990 kHz. The setup enabled localized damage monitoring with 300 mm sensor/actuator spacing and the damage located between the sensor and actuator. A guided waves pitch-catch system was used to monitor a one-meter wind turbine blade during quasi-static testing to failure[17]. An active chirp excitation between 1 kHz - 100 kHz was applied, and the performance of the active vibration system was compared to that of passive mechanical impedance measurements, which can detect local changes in stiffness. The passive mechanical impedance system did not detect damage in the blade, while the active vibration system was able to monitor damage during testing.

During fatigue testing of a 9-meter wind turbine blade, a guided waves pitch-catch system with a frequency range of 5 - 40 kHz was used to detect the initiation and development of a fatigue crack in the root section of the blade[18–22]. A detection range of up to 2 meters was obtained, with the damage not being located between the actuator and the sensor.

From the cited work, it is apparent that high-frequency guided waves systems work well for localized detection of initiation and propagation of damage in wind turbine blades. However, as with the previously mentioned passive high-frequency monitoring systems, a high number of sensors and actuators is necessary for monitoring of large areas of a wind turbine blade, making such systems cost-prohibitive for practical SHM applications.

Accelerometers were used to monitor a wind turbine blade with a length over 40 meters[23]. Propagation of a pressure side shell laminate crack was monitored during fatigue testing. Periodic active excitation was applied in the form of hammer-striking of the blade surface when the fatigue test was paused. A damage index was defined based on the frequency response function transmissibility between accelerometer channels, given a frequency range of 0 - 10 Hz. Step-wise damage propagation was detected during stand-still of the fatigue test.

Buckling of a glass fiber bar was detected through use of an active vibration pitch-catch system[24]. A chirp signal between 60 and 120 Hz was applied to the bar in the undeformed state and at increasing buckling displacements. Buckling of the bar was detected through changes in the measured time series response of the chirp signal. An active vibration pitch-catch system was used to monitor a section of a glass fiber wind turbine blade[25]. By applying a chirp signal with a frequency range of 100 - 500 Hz, simulated damage in the form of added masses was detected through the frequency response function, where peaks shifted frequency as a consequence of the added mass.

An electromechanical actuator was used to actively excite a 34-meter wind turbine blade mounted on a test stand[26]. An array of accelerometers was used to monitor the vibration response resulting from the active excitation. Frequencies above approximately 50 Hz were shown to have a good signal-to-noise ratio as a consequence of the active excitation, and the frequency content above this value was thus useful in terms of blade SHM. An artificial trailing edge debond with a length of 0.2 - 1.2 meters was introduced in the blade. The cross-covariance between accelerometer time series was used as a feature for outlier detection, which enabled detection of the manually induced damage. The previously described active vibration hammer was used on an operating wind turbine with 13-meter blades[27–29]. An artificial trailing edge debond with a length of 0.15 - 0.45 meters was detected by use of the SHM system, which showed the usefulness of active vibration SHM systems for monitoring of blades in operating wind turbines. Further studies on the use of the mentioned active vibration hammer showed feasibility for blade SHM through use of a single accelerometer by exploring the use of different signal processing methods[30].

As presented in the literature review, the presence of relatively severe damage is required to affect detectable changes to the lower-order vibration modes, i.e. within the low-frequency range, of a wind turbine blade. SHM systems relying on monitoring of modal parameters from lower-order vibration modes are as such not necessarily ideal for blades, where detection of smaller, non-critical damages is desirable. While both passive, as well as active high-frequency vibration measurement systems, enable detection of smaller damages, the detection range is very limited. Thus, a high number of sensors is required to cover a larger area of a wind turbine, which results in a cost-prohibitive SHM system. With the purpose of timely detection of damages in wind turbine blades, while keeping the number of necessary sensors at a minimum to reduce costs, SHM systems based on medium-frequency vibrations may present a reasonable compromise between detectable damage size and detection range, as previously reasoned in literature[26]. Hence, the current work seeks to expand on existing research in medium-frequency active vibration monitoring systems for wind turbine blade SHM.

This work is concerned with use of a vibration-based SHM system for monitoring of a commercial 52-meter wind turbine blade subjected to fatigue testing, based on previous work by the authors[14]. Transverse laminate cracks are introduced in the blade sequentially, with progressive damage progression being obtained during fatigue testing, including intermediate repairs of the blade between damages. Applied studies regarding SHM of large structures are not commonly performed, due to availability and costs involved in such test campaigns. However, an important aspect of SHM is its application to real structures, which was the main focus of the test campaign.

Accelerometers are used to measure the vibration response of the blade with active vibration excitation applied by an electrodynamic vibration shaker, which enables accurate control of the frequency content of the applied vibration signal. The medium-frequency range has shown great promise for blade SHM, and as such, the frequency range chosen to be excited by the active vibration shaker is 100 - 3,000 Hz. Damages in the tested wind turbine blade are detected through changes in the medium-frequency vibration response. A damage index is formulated based on the frequency content from acceleration measurements, and statistical outlier analysis is used to quantify changes in the wind turbine blade. The work seeks to showcase the use of an active vibration-based system for SHM of a blade during noisy fatigue testing, with the ultimate purpose of enabling blade SHM for operating turbines. The proposed method enables detection of damages smaller than 0.1 meters within a range of 10 meters in a 52-meter wind turbine blade during fatigue testing.

The section *Wind turbine blade fatigue testing for monitoring of progressive damage development* presents the conducted blade test, the damage cases investigated in this work, a passive vibration monitoring system, and the active vibration-based monitoring system utilized for blade SHM. The signal processing methods used on the collected active vibration data to perform blade SHM are reviewed in the section *Signal processing for vibration-based structural health monitoring*. Results from the data analysis are presented in the *Results* section, showing that damage initiation and propagation can be detected through use of the active vibration monitoring system. Finally, the *Conclusions and discussions* section discusses the findings of this work and draws perspectives on the operational usability of the monitoring system.

Wind turbine blade fatigue testing for monitoring of progressive damage development

The purpose of the present blade test was to collect sensor data with multiple different damages of increasing size, enabling the study of blade SHM. Multiple sensing systems were utilized, as documented by the authors in[14]. The present study focuses on vibration-based methods, investigating both

monitoring of lower-order natural vibration modes as well as a medium-frequency active vibration system.

Blade testing campaign

Wind turbine blades are large, complex structures, and gaining an understanding of the performance of SHM systems for such structures is very important if SHM systems are to gain relevance for use in operating turbines. Concerning studies on the use of SHM systems in large wind turbine blades with progressive damage development, limited research has been conducted, primarily due to limitations set by the financial investment required for such a test campaign.

To work towards the development of an SHM system that can be applied for blades on operating turbines, the authors conducted a full-scale fatigue test of a 52-meter wind turbine blade. The test campaign is at the time of writing unique in multiple ways, in the form of the blade length used, the duration of the test, the number of sensing systems used, the number of damages induced, and finally the repair of damages followed by subsequent testing. Through the investigation of multiple damages, repeatability of the findings from the different sensing systems can be studied, and investigations on feasibility of damage monitoring in different parts of the laminate can also be conducted. The test campaign spanned eight months, in which the blade was instrumented with numerous different sensing systems, including four artificial damage cases introduced in sequence. Through the test campaign, understanding of damage development, as well as damage detection and monitoring in wind turbine blades, was gained, and opportunities and limitations in using different sensing systems for blade SHM were determined.

The test blade used for this work is shown in Figure 1, mounted pressure side up on a test stand at the Siemens Gamesa Blade Test Center in Aalborg, Denmark. A rotating mass fatigue exciter was used to conduct flapwise fatigue testing at the first flapwise eigenfrequency of the blade, which was approximately 0.5 Hz. Fatigue testing was performed with periodic breaks in which the blade was inspected. In terms of excitation applied to the blade, breaks in the fatigue test are denominated stand-still in the following. As such, two different operational states, with very different noise levels, are considered for the blade test: fatigue testing and stand-still, respectively. Moreover, variations in the load applied by the fatigue exciter were observed, which adds to the variability of measurements collected during fatigue testing.

Induced simulated damages

For this work, two manually induced simulated damages are considered, both being cracks in the shear web sandwich panel transverse to the spanwise direction. The shear web is one of the main load-carrying components in wind turbine blades, making it critical for the structural integrity of blades. In a practical application, damage in the shear web may propagate to e.g. the spar cap, which can result in blade failure. From a business perspective, enabling detection and monitoring of such damages through physical and engineering insight is critical for ensuring the structural integrity of wind turbine blades and thus contributing to high uptime of wind turbines.

The first of the investigated shear web damages was initiated through the whole thickness of the shear web sandwich panel at spanwise position 7.5 meters, resulting in the crack shown in Figure 2(a), and Figure 2(b-d) show increased fatigue-driven damage propagation. From the initial crack, a delamination front developed at the crack tip, see Figure 2(b). The delamination propagated at an angle towards the PS spar cap with continued fatigue testing, see Figure 2(c), with the area behind the delamination front cracking through the thickness of the laminate. Figure 2(d) shows the delamination front having grown to a significant size towards the spar cap, and the crack front had also reached the spar cap. At this point, it was decided to terminate fatigue testing and perform repair of the damage.

The second shear web damage, shown in Figure 3, was introduced by cutting through the whole thickness of the face sheets of the shear web at spanwise position 9 meters. For the same damage, zoomed-in views of zones with fatigue-driven damage propagation are shown in Figure 4. The damage was induced manually at an initial length of 30 mm, followed by sequential manual increases in length of 60, 90, and 400 mm, respectively. With lengths between 30 and 90 mm, propagation of the damage during fatigue testing was limited to small areas with delaminations at the crack tips. Due to the limited propagation, it was decided to perform manual increases in length. With the final manual increase in length of 400 mm, damage propagation during fatigue testing was more significant than previously, resulting in cracking all the way through the shear web laminate, see Figure 4(c). At the crack tip towards the spar cap, a delamination developed and eventually grew to the spar cap, see Figure 4(b). At this point, it was decided to stop fatigue testing and repair the damage. The positioning of both shear web damages is sketched in Figure 8.

Passive vibration monitoring system

One of the sensing systems used in the blade test campaign was a distributed accelerometer system, consisting of 22 triaxial micro-electromechanical systems accelerometers distributed on the leading edge (LE) and trailing edge (TE) of the blade, as shown in Figure 5. Acceleration data was sampled continuously at 250 Hz, and the purpose of the sensing system was to investigate the feasibility of detecting the induced damages through changes in the lower-order natural vibration modes of the blade. From the literature [11,13], it has been shown that the lower-order natural vibration modes of a wind turbine blade were not sensitive to the presence of a trailing edge debond. In the course of the blade test, it was investigated if the induced shear web damages cause changes in the lower-order natural vibration modes, as previously documented by the authors [14].

To extract the natural vibration modes of the blade, OMA was performed using the acceleration data. In this case, a correlation-function-based stochastic subspace identification algorithm was used [31–33].

A stabilization diagram extracted using OMA is shown in Figure 6. Natural vibration modes of the blade up to approximately 9 Hz can be estimated with good modal separation, while modes at frequencies higher than this

Figure 1. Wind turbine blade mounted on a test stand at Siemens Gamesa Blade Test Center in Aalborg, Denmark.

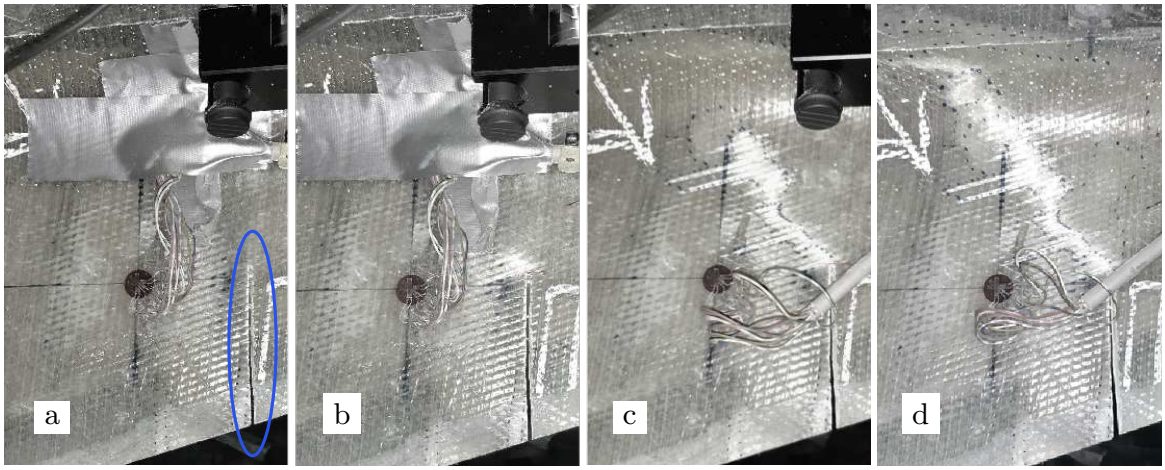

Figure 2. First shear web damage with an initial length of 100 mm, marked with a blue ellipsis (a), followed by progressive fatigue-driven damage propagation (b-d). Areas with delaminations were manually marked with dots.

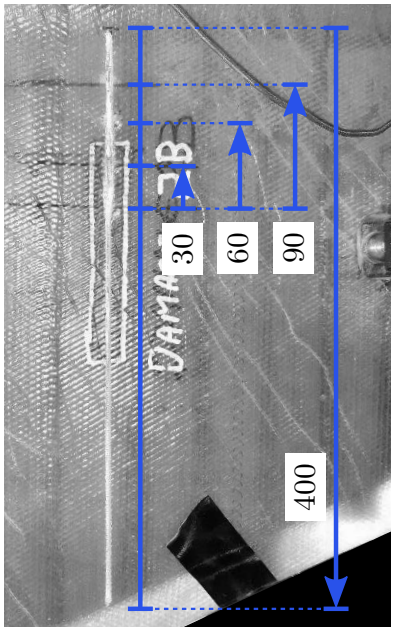

Figure 3. Second shear web damage with initial length of 30 mm, followed by three sequential manual increases in length.

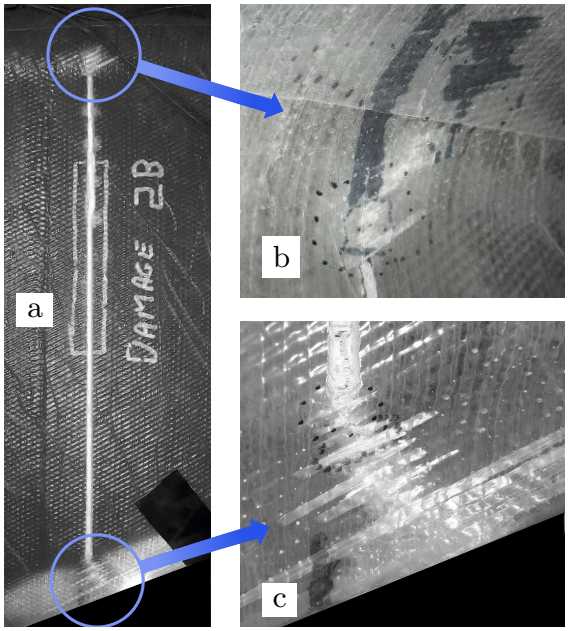

Figure 4. Second shear web damage, showing final length with damage growth during fatigue testing.

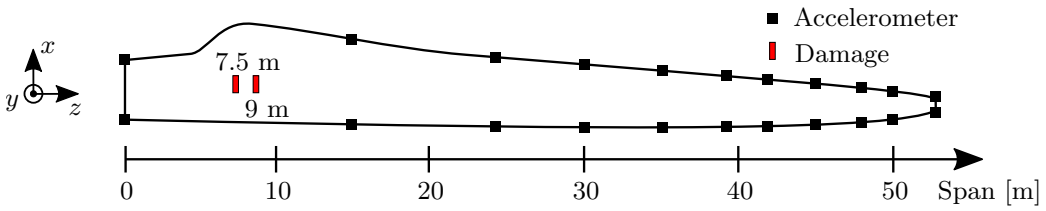

Figure 5. Low-frequency accelerometers distributed along the span of the blade on the LE and TE.

become increasingly difficult to separate. Thus, OMA is deemed to be most useful for estimation of the lower-order vibration modes of the blade. Comparing the eigenfrequencies of the first seven natural vibration modes of the blade, differences found between eigenfrequencies in the healthy and damaged states of the blade were generally below 1%, which is deemed to be too small of a change to be detectable in practical applications. Likewise, for the mode shapes associated with these vibration modes, there were no significant differences between the healthy and damaged states. As such, it was concluded that the lower-order natural vibration modes of the blade would not serve as reliable features for detection of small damages in wind turbine blades.

SHM of wind turbine blades using passive vibration monitoring based on OMA with ambient excitation is deemed to provide too coarse resolution in terms of detectable damage size since a damage detectable through OMA will need to significantly affect the lower-order vibration modes of the blade. Thus, the damage will need to significantly affect the global stiffness of the blade, at which point such a damage is deemed to significantly affect the structural integrity of the blade. At that point, critical blade failure would most likely be imminent. As such, it is desired to detect damages at a much earlier stage, where costs associated with the damage are limited to repair costs and temporary loss in energy production during repair.

Having shown that monitoring of modal parameters through ambient vibration excitation is not sufficiently sensitive for detection of small damages in wind turbine blades, this form of passive vibration monitoring is not a reliable method for blade SHM. Thus, a more sensitive monitoring system, providing finer resolution in terms of detectable damage size, needs to be designed. This is addressed in the remainder of the paper through an active vibration monitoring system combined with statistical analysis.

Active vibration monitoring system

To facilitate SHM of wind turbine blades, the previous section shows that low-frequency passive vibration systems, such as systems relying on natural vibration modes, are not reliable for detection of damages in due time before they become critical to the structural integrity of blades. As such, it has been proposed to employ active vibration systems, which ideally provide an appropriate compromise between monitoring range and detectable damage size. The active vibration monitoring system used in this work is shown mounted inside the test blade on the shear web laminate in Figure 7. The active vibration monitoring system consists of an electrodynamic vibration shaker (Dewesoft DS-IS-40, frequency range 10 - 3,000 Hz), a colocated force transducer (Dytran 1053V1), and 11 uniaxial accelerometers (Brüel & Kjær type 4507-B-006, frequency range 0.2 - 6,000 Hz). Signal generation and data acquisition is handled with an NI cDAQ-9185 data acquisition unit, three NI-9234 input modules, and one NI-9260 output module, controlled through a laptop PC with MATLAB software. The vibration shaker was mounted on the blade laminate by use of a steel mounting plate, which was adhered to the surface of the blade laminate. The force transducer was mounted in between the vibration shaker and the mounting plate. The accelerometers were mounted with plastic mounting plates, which were adhered to the blade laminate.

Between repair of the two shear web damages, the vibration shaker had to be moved from its initial position. Thus, the location of the active vibration input is not the same for the data available for the two damage cases presented in this work, and the measurements from the repaired state cannot readily be compared to the baseline healthy state or the damaged state of the first shear web damage.

Placement of the shaker, accelerometers, and damages are sketched in Figure 8. Accelerometers sketched in white were located on the shear web laminate, and accelerometers sketched in blue were located on the TE shell laminate, see Figure 9 for a sketch of the three-dimensional blade view showing the accelerometer locations. The damages and the vibration shaker were placed on the PS side of the shear web. The accelerometers placed on the shear web were also placed towards the PS side, while the accelerometers towards the TE were placed on both the PS and SS side shell laminate. The active vibration input of the electrodynamic vibration shaker and measured output from an accelerometer are plotted in Figure 10. A logarithmic sinusoidal chirp with frequencies between 100 and 3,000 Hz is applied over a time of 12 seconds, with a period of no input at either end of the signal. This frequency range is well above that of the lower-order eigenfrequencies of the blade. White noise and sinusoidal burst signals were also applied, but these signals are not investigated in the present work. The sinusoidal chirp signal is selected for the present study due to its high signal amplitude and wide frequency range. A sampling frequency of 25,600 Hz is used for the accelerometers and for the force transducer. The logarithmic chirp time domain response as a function of time t is governed by Equation (1) and (2):

$$x(t) = \cos\left[2\pi f_0 \left(\frac{k^t - 1}{\ln(k)}\right)\right] \tag{1}$$

$$k = \left(\frac{f_1}{f_0}\right)^{\frac{1}{T}} \tag{2}$$

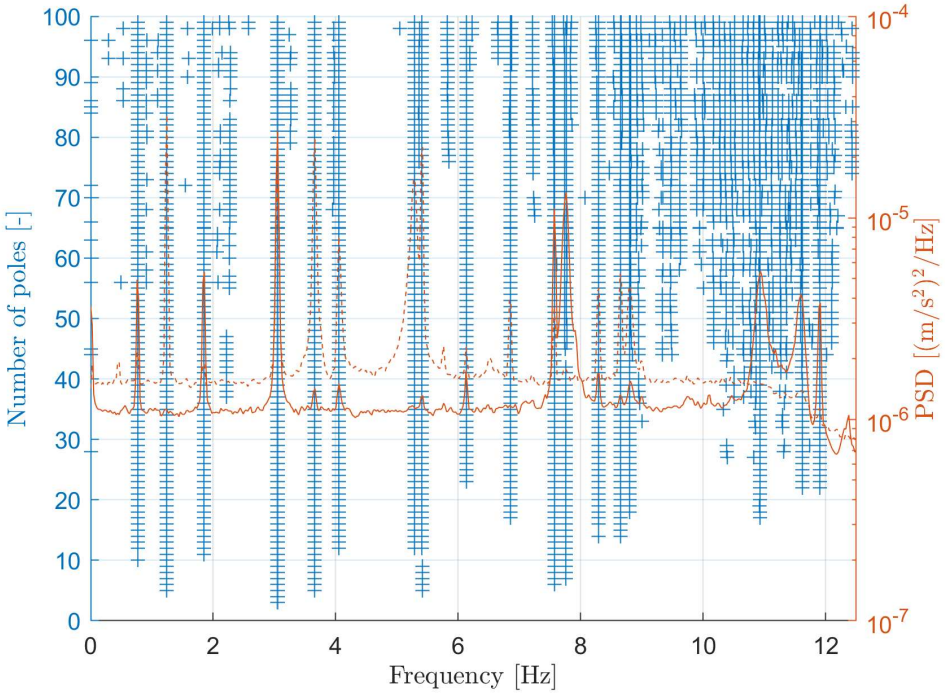

Figure 6. Stabilization diagram extracted with OMA using data from the distributed accelerometers shown in Figure 5, as previously presented by the authors[14]. Stable poles are marked with crosses; unstable poles are not shown. Solid and dashed orange lines show the Welch PSD estimate of the flapwise and edgewise acceleration signals, respectively.

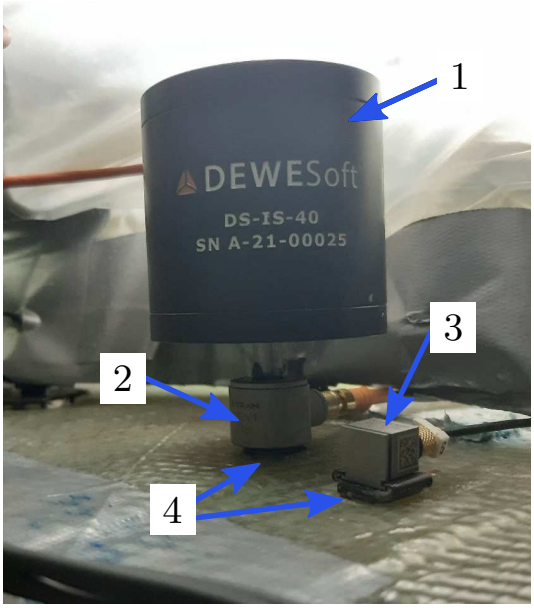

Figure 7. Electrodynamic vibration shaker (1) mounted on shear web laminate inside wind turbine blade, colocated force transducer (2), accelerometer (3), and mounting plates (4).

where f_0 and f_1 are the starting and ending frequencies, respectively, and T is the duration of the logarithmic chirp signal. The frequency response of the chirp at a given time t is defined in Equation (3):

$$f(t) = f_0 k^t \tag{3}$$

The input force from the vibration shaker, measured with the colocated force transducer during stand-still of the blade test, is plotted in Figure 10(a), and the associated frequency response is shown in the spectrogram in Figure 10(b). The resulting output acceleration, measured by accelerometer 9, see Figure 8, is plotted in Figure 10(c), and the associated frequency response is plotted in Figure 10(d). For the case of fatigue testing, the output acceleration measured during shaker excitation and the associated frequency response is plotted in Figure 10(e) and 10(f), respectively. Comparing the frequency responses from the operational states of stand-still and fatigue testing, Figure 10(d) and 10(f), respectively, it is apparent that fatigue testing adds additional noise to the frequency response, partly in the form of harmonics and higher-order harmonics of the fatigue excitation frequency, with the frequency input of the chirp signal still being distinguishable. The mean signal-to-noise ratio for accelerometer 9 across the entire utilized frequency range is 56 dB during stand-still and 26 dB during fatigue testing.

Signal processing for vibration-based structural health monitoring

The steps taken from time series data to quantification of the health state of the blade are presented in the following.

Data cleansing

The noise floor in an operating turbine was investigated in[26], where the noise magnitude exhibited a steep decline between 0 and 100 Hz. The noise observed during fatigue testing in the present study is much in line with the observations from the cited work, with the noise magnitude during fatigue testing exhibiting a large decline between 0 and

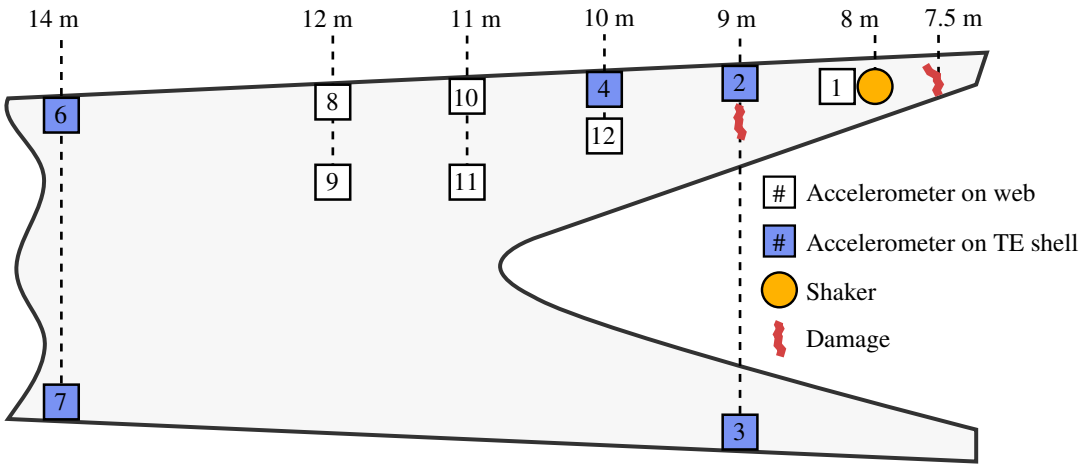

Figure 8. Accelerometer channel placement on shear web and shell laminate, viewed from trailing edge side. Sensor channel 5 is used for the force transducer, which is colocated with the vibration shaker. The first shear web damage, shown in Figure 2, is located at 7.5 m, and the second shear web damage, shown in Figure 3 and 4, is located at 9 m.

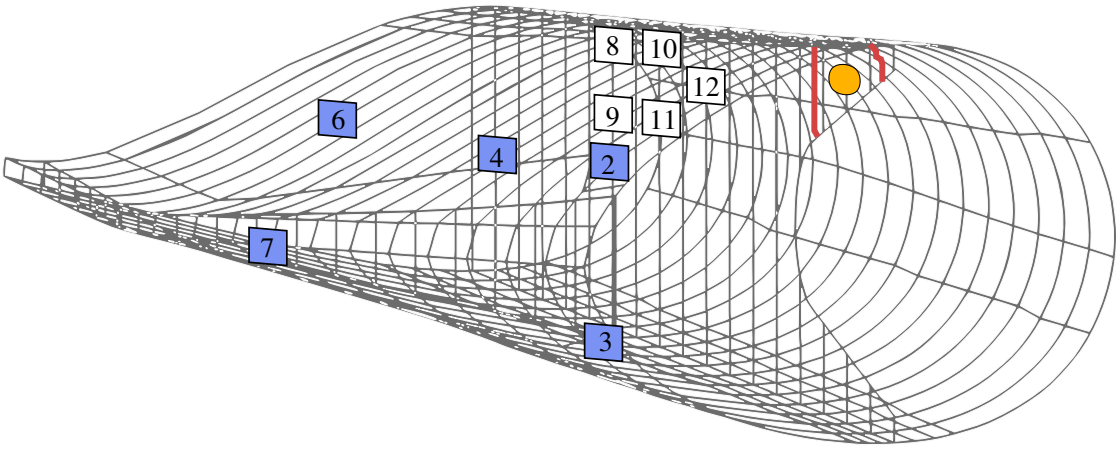

Figure 9. Accelerometer channel placement illustrated on three-dimensional view of wire-frame blade model, showing spanwise location 6 - 15 meters. Accelerometers 2-4, 6, and 7 are placed on the shell laminate towards the TE; accelerometers 8-12 are placed on the shear web laminate. Coloring of accelerometer channels, shaker, and damages is equivalent to that in Figure 8.

200 Hz, see Figure 11. For e.g. accelerometers 6 and 7, which are the sensors placed furthest from the vibration shaker in the present work, the measured amplitude of the vibration shaker signal attenuates more. For the mentioned sensors, frequencies below approximately 500 Hz show higher noise amplitudes than the measured shaker signal, whereas for frequencies above approximately 500 Hz, the noise amplitude is lower than the measured shaker signal.

The attenuation of the shaker signal is investigated by plotting the vibration amplitude, normalized by the amplitude of the accelerometer placed right next to the vibration shaker (accelerometer channel 1), at different frequencies as a function of the approximate distance from the vibration input, shown in Figure 12. The used distance takes into account both the spanwise and chordwise placement of the accelerometers, see Figure 8 and 9. In general, there is no monotonic attenuation observable, which is deemed to be due to vibration amplitudes at specific frequencies being amplified by local vibration modes.

Feature selection and extraction

To enable quantification of the health state of a structure, it is necessary to determine and extract damage-sensitive features from the original time series data recorded during testing with the structure. Using the raw time series data would not be computationally efficient in an operational application, nor would it offer good performance with regards to damage detection, due to inherent randomness in the time series data[34]. If damage-sensitive features are selected, changes in the health state of the structure will be easier to find, and the changes may even be visible directly from the damage-sensitive features. Ideally, these features are insensitive to operational and environmental variability, but this is not the case in most operational applications[35]. Moreover, if critical damages are detected, they will likely require repair. Such externally introduced structural changes will also alter the structural response of the structure, compared to the healthy baseline as well as the damaged state before repair of the damage. Being able to account for such changes also needs to be considered.

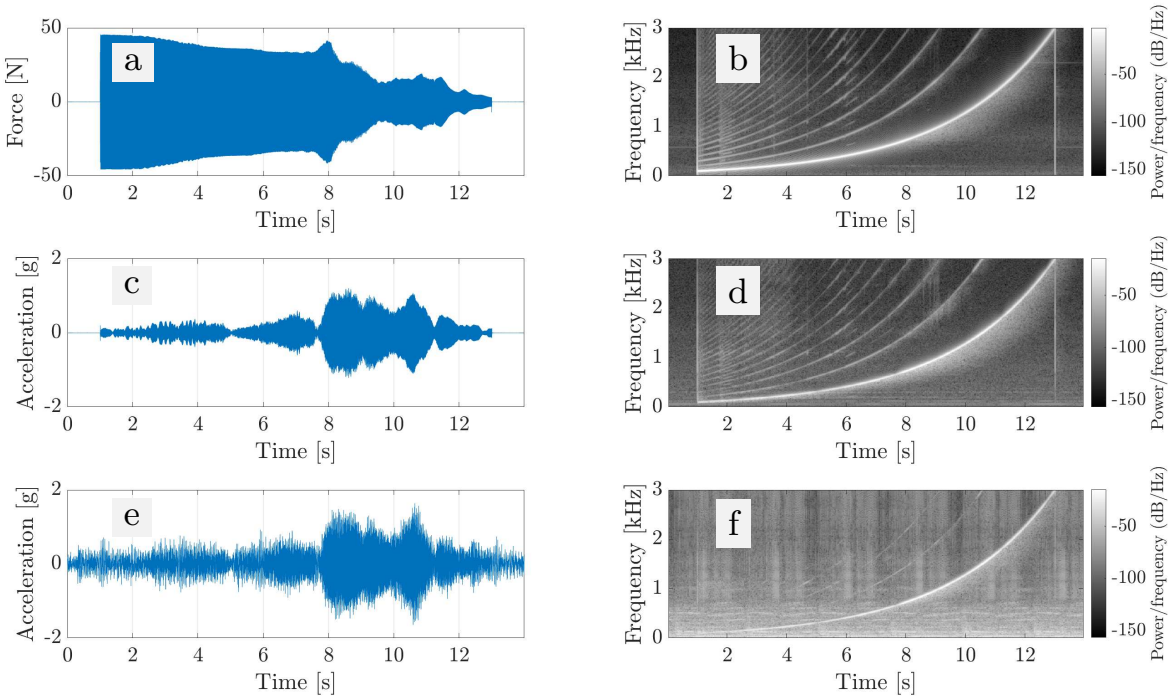

Figure 10. Logarithmic sinusoidal chirp vibration input: Force input time series measured with colocated force transducer (a), frequency response of force input (b), time series of acceleration response measured with accelerometer 9 (c) and associated frequency response (d) during stand-still, as well as time series of acceleration response measured with accelerometer 9 (e), and associated frequency response (f) during fatigue testing.

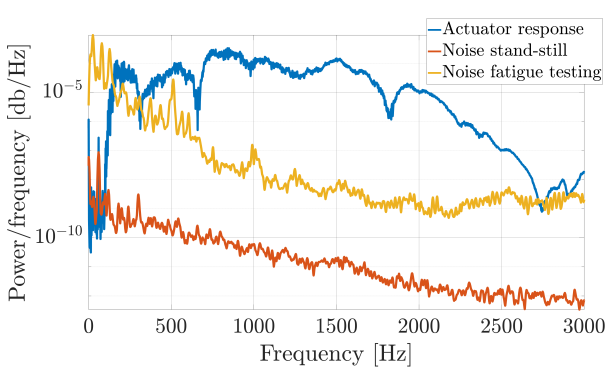

Figure 11. Comparison of PSD of chirp signal vs. PSD of noise floor. Based on acceleration measurements of accelerometer 9, see Figure 8.

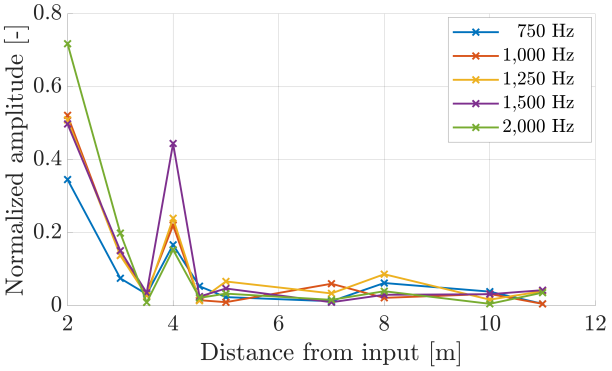

Figure 12. Vibration signal attenuation at different frequencies, normalized by the amplitude of the acceleration output measured by accelerometer channel 1, see Figure 8.

The available time series data, i.e. the accelerometer output recorded during excitation with the vibration shaker, is sampled at 25,600 Hz over a period of 14 seconds, which can be reduced to 12 seconds, corresponding to the length of the chirp signal. With 12 measurement channels, this corresponds to 307,200 by 12 data points for each observation recorded during testing. Features sensitive to changes in the physical response of the blade caused by the initiated damages are desired to be found. In this work, the features used for studies on blade SHM are the frequency response calculated from the accelerometer outputs. The damages initiated in the blade laminate are believed to affect the local stiffness and thus the local vibration response of the blade laminate, which will alter the local frequency response. Towards this purpose, the Welch power spectral density (PSD) estimate is used to calculate the frequency response from the accelerometer output. This PSD estimator is chosen, since its definition may reduce the variance of the estimated PSD, compared to e.g. the periodogram estimator[36].

For use in SHM, the PSD estimate will, depending on the choice of parameters for the Welch PSD formulation and the FFT algorithm, have a much lower number of data points than the original time series data. For this work, the number of data points is reduced from 307,200 by 12 in the time domain to 3,481 by 12 in the frequency domain through the process of feature selection and extraction.

Dimensionality reduction To increase computational efficiency, the dimensionality of the feature space is commonly reduced. Methods of dimensionality reduction are available, which retain a large percentage of the original data, while significantly reducing the dimensionality of the data. One popular method of dimensionality reduction is

principal component analysis (PCA), in which an orthogonal projection of the original data X onto a space with lower dimensionality is performed, maximizing the variance of the projected data W, see e.g.[37]. This is commonly done through linear projection:

$$W = XV \tag{4}$$

where V contains the principal component directions, which can be obtained through e.g. singular value decomposition (SVD) of the original data:

$$X = USV^T \tag{5}$$

where the columns of U and V are referred to as the left and right singular vectors, respectively, and S is a rectangular diagonal matrix containing the singular values of X. The right singular vectors of V and the singular values in S can be shown to be related to the eigenvectors and eigenvalues of X, respectively, which enables the use of SVD for calculation of principal components[38]. Commercial software often uses SVD in PCA, instead of e.g. eigenvector factorization, due to increased computational efficiency and reduced numerical difficulties for real data sets[37].

The principal components are calculated in descending order of percentage of the variance explained, i.e. the first principal component will be the direction of maximum variance, followed by the second principal component, and so on. To ensure that the principal components are calculated in decreasing order of percentage of the variance explained, it is necessary to demean the original data such that:

$$X = X_o - \overline{X}_o \tag{6}$$

where X is the demeaned data, on which PCA is performed, X_o is the original data, and $\overline{X}_o$ is the mean of the original data.

Outlier analysis

To monitor the health state of the tested wind turbine blade, outlier analysis is conducted by use of a discordancy test. The purpose of this work is to demonstrate the application of a novel sensing system applied for blade SHM. As such, a classic discordancy test, in form of the Mahalanobis distance, is used. The Mahalanobis distance is a multivariate generalization of the Euclidean norm, which is commonly used as an outlier detector in SHM, see e.g.[26–28,34]. The Mahalanobis distance is defined as:

$$D_i = \sqrt{(y_i - \overline{X})^T S^{-1} (y_i - \overline{X})} \tag{7}$$

where y_i is the i$^{\text{th}}$ observation of the testing data Y, in which potential outliers are searched for, $\overline{X}$ is the mean of the training data X, and S is the covariance of the training data X. The Mahalanobis distance serves as a discordancy test, which thus determines whether the observation y_i is an outlier from the training data X. In terms of blade SHM, the training data X will be sampled during the healthy state of the blade, and potential outliers in the testing data Y, caused by changes to the structural integrity of the blade, are desired to be detected. Based on the training data X, corresponding to the healthy state of the blade, a discordancy value D_0, also referred to as confidence interval, is calculated. In this work, the approach proposed in[34] is used, wherein the discordancy value is calculated in an inclusive manner, based on a number of random trials, which are calculated from the mean $\overline{X}$ and covariance S of the training data X. The discordancy value D_0 is chosen based on the $(100 - F)$th percentile of the random trials, corresponding to $F\%$ false positives, classifying the healthy trials as false outliers, i.e. states of damage.

To classify all observations in the potential states of healthy or damaged, damage indices D_i for all observations y_i in the testing data Y are calculated. Based on each value of the damage index D_i, the state for the corresponding observation y_i is classified as healthy or damaged based on whether or not it is an outlier when compared to the discordancy value D_0. Hence, $D_i \leq D_0$ is classified as healthy, while $D_i > D_0$ is classified as damaged, given the specified confidence interval.

Since the blade test campaign was conducted inside a temperature-controlled hall, environmental conditions such as temperature are kept relatively constant, compared to external conditions. Thus, environmental variations need not be accounted for, and outliers detected in connection with damaged observations are deemed to be due to changes in the health state of the blade.

Results

First shear web damage: spanwise location 7.5 meters

Feature extraction and dimensionality reduction: Based on the data recorded during stand-still and fatigue testing of the wind turbine blade, use of the active vibration monitoring system for blade SHM is studied. A total of 5,791 observations are available with the logarithmic chirp input for the damage case shown in Figure 2, with 3,076 and 2,395 being in the healthy and damaged state, respectively. For the available observations, the PSD is calculated for the frequency range of the chirp signal. The PSDs corresponding to all available observations from accelerometer 9 are plotted in Figure 13. Following the manual introduction of the shear web damage, a jump in PSD magnitude can be observed at multiple frequency ranges. This may indicate that the local vibration response of the shear web laminate is altered due to the stiffness reduction which results from the shear web crack. Additionally, progressive change in the PSD magnitude with increasing damage severity can be observed for multiple frequency ranges, which may indicate that the progressive damage growth obtained during fatigue testing results in progressive changes to the local vibration response of the shear web laminate.

Upon more detailed inspection of the PSDs from the available measurement channels, differences between stand-still and fatigue testing are most prevalent below approximately 600 Hz. Additionally, the PSD magnitude decreases significantly above 2,500 Hz. As such, the frequency range used for outlier analysis is trimmed to the range between 600 and 2,500 Hz.

Regarding dimensionality reduction with PCA, choosing the number of principal components (PCs) to be used is

not trivial, since the signal-to-noise ratio between the active vibration signal and noise present during fatigue testing varies for the available sensor channels, being dependent on the distance to the active vibration input as well as the location of the sensor placement, e.g. on the shear web or spar cap laminate. The closer the sensor channels are located to the active vibration input, the fewer PCs are necessary for separation between healthy and damaged states as well as for evaluation of the damage severity. The first two PCs, calculated from the PSD data from all accelerometer channels, are plotted in Figure 14. It can be observed that the first PC provides separation between the healthy and damaged states for channels 1, 3, 4, and 9 - 12, while a combination of the first and second PC yields separation between the healthy and damaged states for channel 8. For the remaining channels, a higher dimensionality of PCs is required to separate the healthy and damaged states. For channels 1, 11, and 12, the second PC exhibits, to some degree, monotonic change in line with the gradual progression of the damage severity, and this PC thus yields information regarding the damage severity for the listed channels. Higher dimensionality is necessary for the remaining channels to extract information on progression of the damage severity.

To ensure that choice of the number of PCs to be used as features for outlier detection is made on an informed basis, a study on the effect of the number of PCs on the classification accuracy is conducted. For this study, both the PSD data with the trimmed frequency range of 600 - 2,500 Hz as well as the full available frequency range of 100 - 3,000 Hz is used to highlight the effect on classification accuracy when removing the part of the frequency range with lower signal-to-noise ratio. The results of this study are shown in Figure 15, where the classification accuracy and percentage of variance explained are plotted as a function of the number of PCs for all accelerometer channels. In general, most of the healthy training and test observations are classified correctly with a single component for all the accelerometer channels, which yields a classification accuracy just above 50%. For the accelerometer channels placed close to the damage, e.g. channels 9 - 12, trimming the frequency range to 600 - 2,500 Hz does not make a significant difference in the classification accuracy. However, for the accelerometer channels placed further from the damage, e.g. channels 2 and 7, the performance is generally increased by trimming the frequency range to 600 - 2,500 Hz. By comparing the percentage of variance explained of channel 7 for the two different frequency ranges, it can be observed that a larger percentage of the variance is explained when retaining the full frequency range of the input signal, while the classification accuracy is lower, compared to the case of the trimmed frequency range.

A study on the use of frequency lines from the PSDs, within different frequency ranges as features, was also conducted. General observations are as follows:

- Using wider frequency ranges as features, e.g. 150 Hz, corresponding to 200 frequency lines, resulted in poor performance, likely due to the inclusion of random noise.
- Using frequency lines below 600 and above 2,500 Hz yielded poor performance, as discussed previously.
- Using approximately 100 frequency lines, corresponding to a frequency range of 65 Hz, in the range 600 - 2,500 Hz, generally yielded good performance.
- Shifting the frequency range by e.g. 50 Hz could make the difference in whether or not a change in the damage index coincident with the development of damage is detected. This is most likely due to specific frequencies being altered as a consequence of damage initiation and propagation. Whether or not these frequencies are included in the feature space makes the difference between being able to detect both initiation and propagation of damage. As such, the method is very sensitive to the choice of frequencies used.
- Progression of the damage index in line with damage progression displays many variations depending on the utilized frequency range. This may also indicate that different frequencies are exhibiting changes at different stages in the progression of the damage.

A closer investigation of the sensitivity of the damage index to different frequency ranges may yield more physical understanding of the effect of a damage on the local vibration response of the structure. However, if no prior knowledge is available of which frequencies are affected by damage, using PCA is a much more time-efficient and reliable way to perform feature extraction.

For detection of damage in the present study, PCs explaining 95% of the variance of the original PSD data in the frequency range 600 - 2,500 Hz are used. The corresponding number of PCs for each accelerometer channel is listed in Table 1. Generally, the number of PCs required to explain 95% of the variance is lowest for the accelerometer channels placed on the shear web laminate closest to the vibration shaker, e.g. channels 1, 9, 11, and 12. For the accelerometer channels placed further away on the shell laminate, e.g. channels 2 and 7, the number of PCs required to explain 95% of the variance is much higher. This is most likely due to the signal-to-noise ratio decreasing with increasing distance from the active vibration input as well as the measured signal being dependent on the laminate thickness and fiber orientation in the laminate.

Table 1. Number of PCs required to explain 95% of the variance of the original data for all accelerometer channels, used as features for outlier detection.

Accelerometer channel number	Number of PCs explaining 95% of the variance
1	5
2	38
3	23
4	34
6	13
7	42
8	23
9	8
10	24
11	5
12	10

Detection of initiation and progression of damage: Using the extracted features, outlier analysis is performed to enable

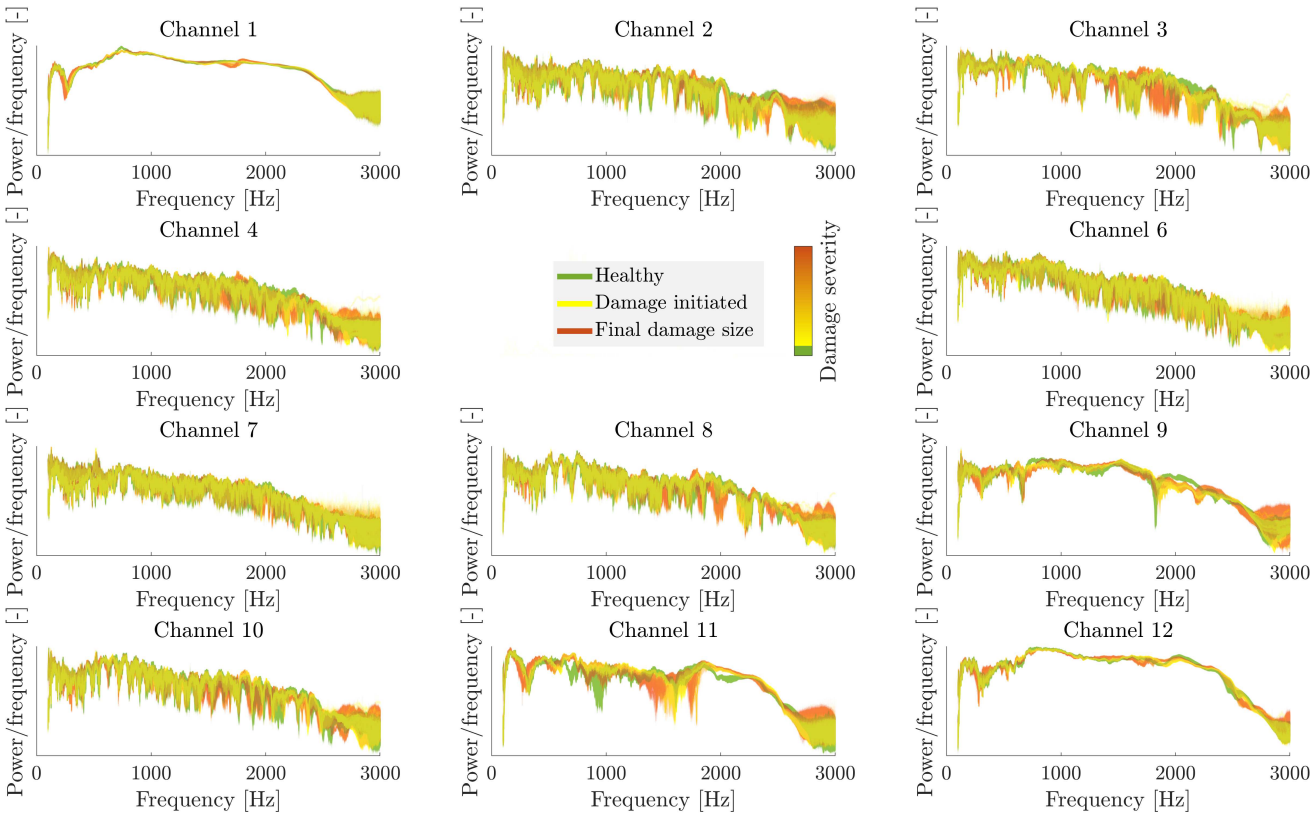

Figure 13. PSDs from all accelerometer channels (see Figure 8) resulting from active vibration input, plotted for all observations recorded during testing with the first shear web damage. Observations recorded during the healthy state of the blade are plotted in green, while observations starting after the manual initiation of the damage are plotted on a yellow to red color scale with increasing damage severity. Overlap renders as mixed colors.

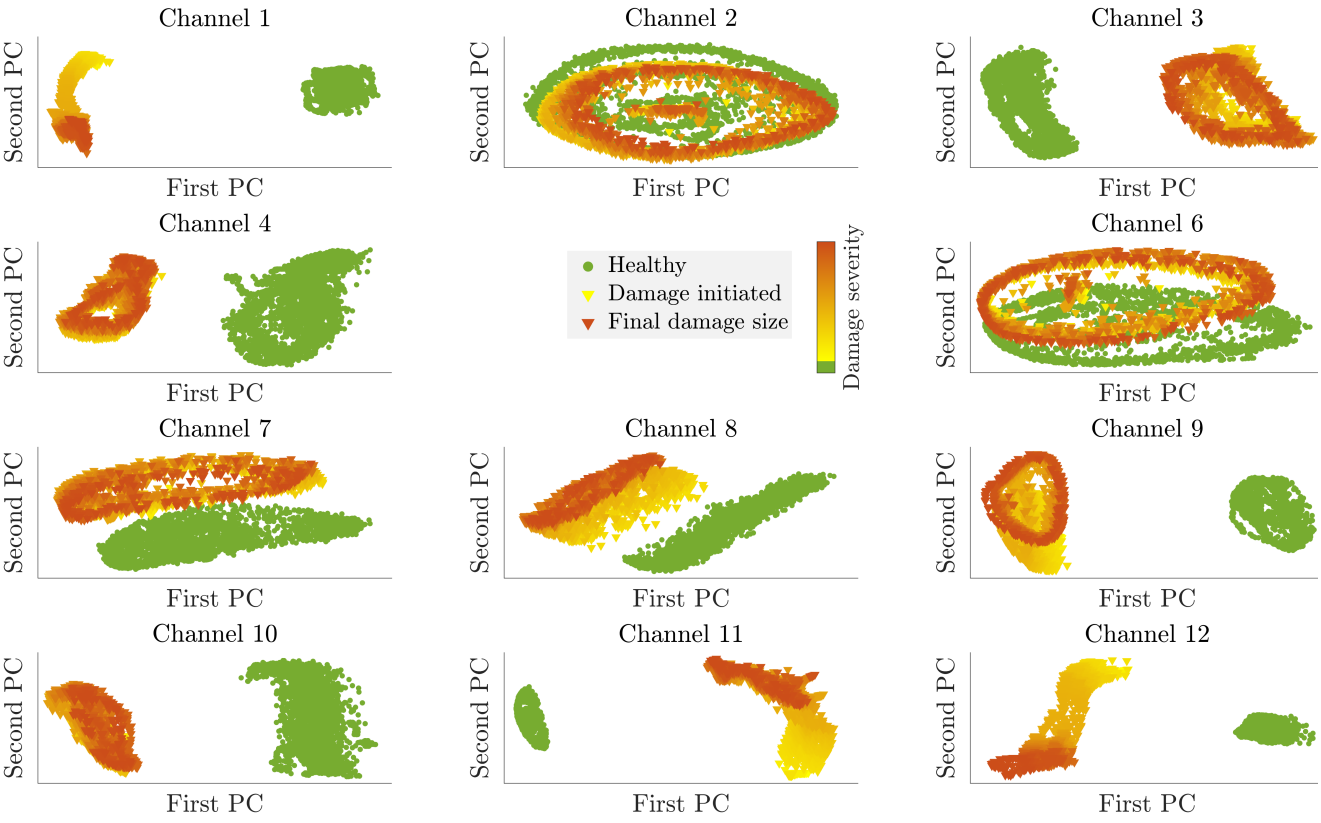

Figure 14. First two PCs for the PSD data from all accelerometers, using frequencies between 600 and 2,500 Hz. Healthy observations are plotted in green, while damaged observations are plotted on a color scale from yellow to red with increasing damage severity.

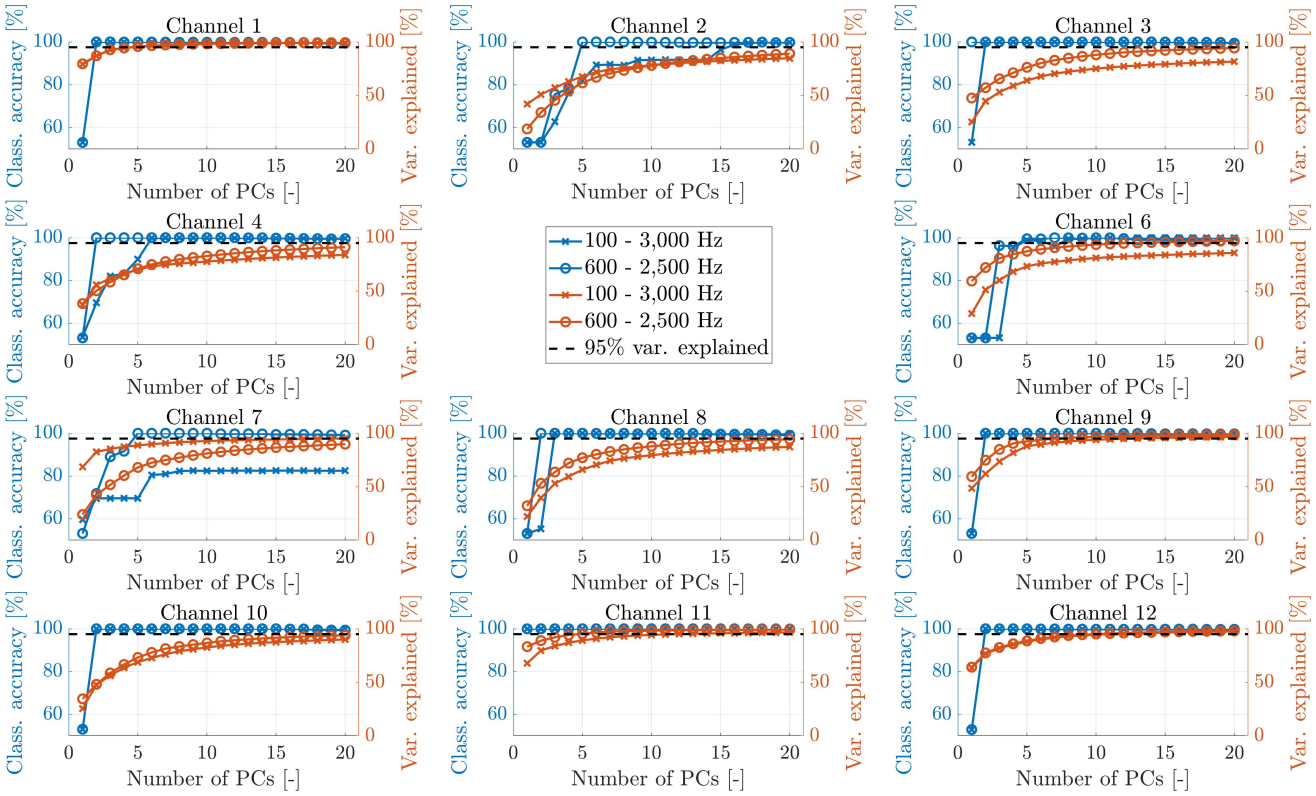

Figure 15. Classification accuracy (Class. accuracy) and variance explained (Var. explained) as a function of the number of PCs, plotted for all accelerometer channels, both using the full frequency range of 100 - 3,000 Hz as well as the trimmed frequency range of 600 - 2,500 Hz. It should be noted that the lower limit of the second axis depicting classification accuracy is set to 50% for all accelerometer channels.

detection of the shear web damages. Figure 16 shows outlier plots for all accelerometer channels, using data recorded during testing with the shear web damage shown in Figure 2. The Mahalanobis distance, see Equation (7), is used for discordancy testing, and the healthy threshold is calculated with a 99% confidence interval based on every second observation from the first 90% of the healthy data. Generally, for all accelerometer channels, more than 99% of the healthy observations are classified as inliers, while all damaged observations are classified as outliers. A large jump in the damage index D can be observed after the introduction of the shear web damage, followed by progressive change in the damage index in line with the observed damage progression. However, progression in the damage index is not monotonic for all accelerometer channels, and neither does the damage index increase in magnitude with increasing damage severity for all accelerometer channels. For e.g. channels 7 and 10, the progressions after damage initiation are close to mirror images of each other. For channel 7, the damage index increases monotonically in line with progression of the damage, whereas the damage index decreases monotonically with progression of the damage for channel 10. Whether or not the damage indices increase monotonically with increasing damage severity is believed to be dependent on whether the positions of the corresponding accelerometers are sensitive to the changes in the local vibration response resulting from damage, as well as the number of PCs used as features for outlier detection.

Considering channel 10, the damage index decreases monotonically with increasing damage severity. One possible explanation for this is the local vibration response of the blade changing towards resembling the vibration response at the healthy baseline, as compared to becoming more different from the vibration response after introduction of the damage. Similar behavior, where the damage index partially decreases with increasing damage severity, can be observed for other accelerometer channels. Since damages in e.g., glass fiber reinforced epoxy do not repair themselves, changes in the damage index over time are indicative of changes in the damage state in form of damage propagation.

Another observation that can be made from the plots of the damage indices is the presence of distinct zones in the observations from the damaged states. For the plot from channel 4 in Figure 16, the observations following initiation of the damage are shown in Figure 17. The observations in the first block marked with dotted blue lines in Figure 17 have little variance, followed by a second block of observations marked with blue dotted lines, where the observations have increased variance. These two types of blocks are repeated throughout the damaged observations. The consecutive observations with little variance were sampled during stand-still of the fatigue test, whereas the consecutive observations with increased variance were sampled while the fatigue test was running. Consequently, the noise from fatigue testing adds variance to the damage index, which may be due to e.g. opening and closing of the crack during fatigue testing. Observations from both the operational states of stand-still and fatigue testing are classified correctly as outliers since both of these operational states were included in the training data.

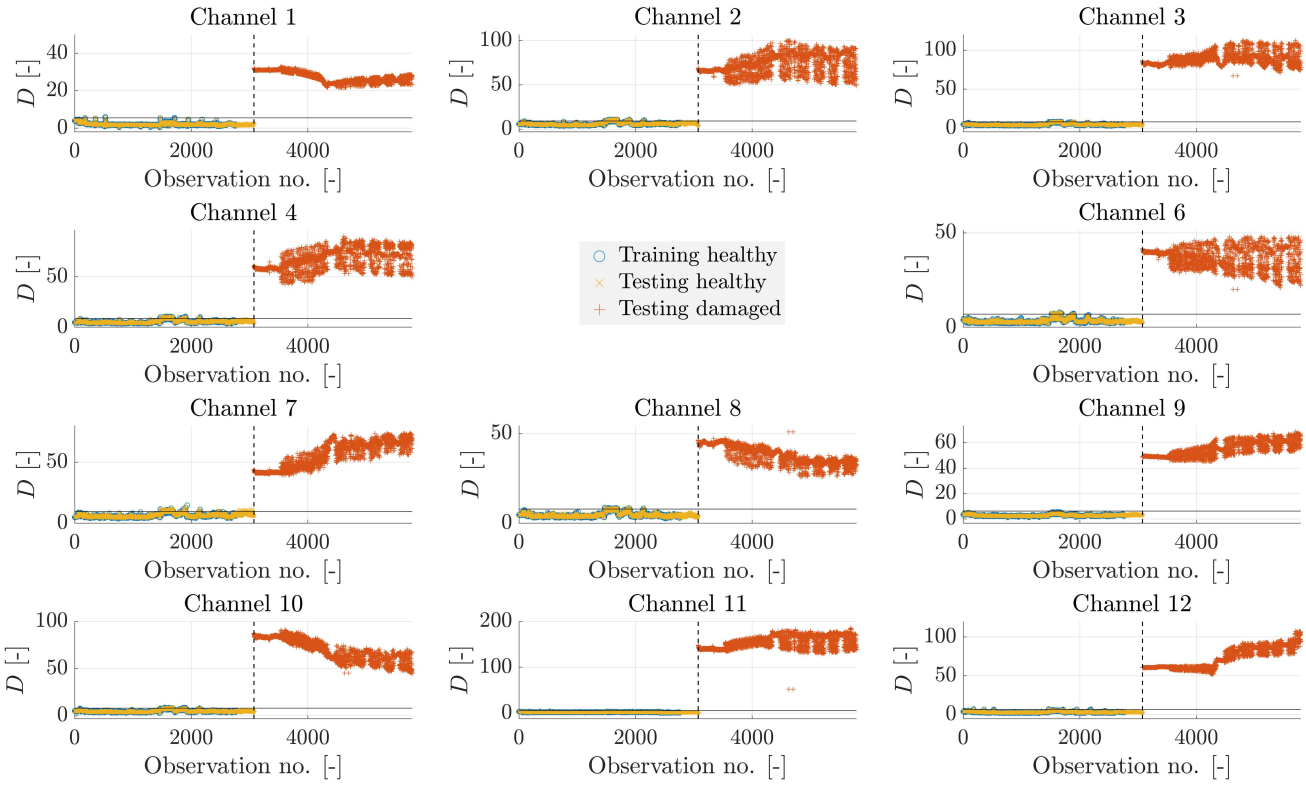

Figure 16. Plot of damage index D, calculated based on the Mahalanobis distance by using PCs explaining 95% of the variance of the original data. The horizontal solid line marks the 99% confidence threshold, allowing for 1% false positives in the training data. The vertical dotted line marks the manual introduction of the first damage.

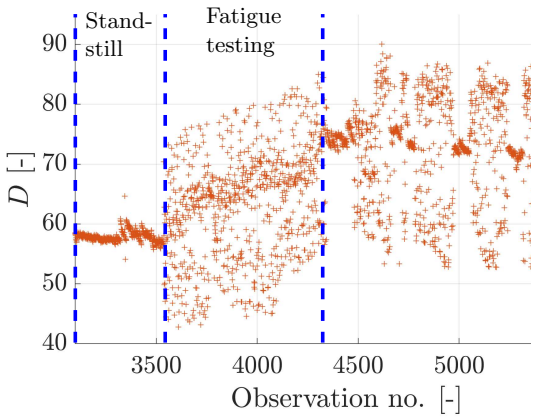

Figure 17. Zoomed-in view of damaged observations of channel 4 from Figure 16.

Second shear web damage: spanwise location 9 meters

Feature extraction and dimensionality reduction: In line with the previously treated damage case, data is available from the operational states of stand-still and fatigue testing for this damage case. The number of observations available for each health state with the present damage case is listed in Table 2. As opposed to the previously presented data, multiple lengths of manual damage increase are available for this damage, including fatigue-driven damage propagation, which was mainly occurring after the manual increase of the damage length to 400 mm. The procedure used for feature extraction and dimensionality reduction is the same as previously presented: Trimming of the frequency range of the PSDs to 600 - 2,500 Hz and using PCA dimensionality reduction, employing PCs corresponding to 95% of the variance explained. To get an overview of the features to be used for outlier analysis, the first two PCs for all accelerometer channels are plotted in Figure 18. Generally, two PCs are not adequate to yield separation between the healthy and damaged states, and neither can most of the damaged states be separated. For channels 1 and 8 - 12, there is clear separation for the damaged state with 400 mm crack length. Additionally, for channels 9 - 12, the observations for the damaged state with 400 mm crack length seem to be separable into two clusters, most likely being observations before and after the damage propagated all the way through the shear web laminate, see Figure 4(a,c), which is believed to significantly alter the local vibration response of the shear web laminate.

Table 2. Number of observations available for the second shear web damage at the investigated health states.

Health state	Number of observations
Healthy	669
30 mm	496
60 mm	778
90 mm	675
400 mm	3,523

The classification accuracy and percentage of variance explained as a function of the number of PCs are also studied for the second damage, see Figure 19. Classification accuracy is much lower with a single PC compared to the

first damage, which most likely stems from the fact that the percentage of healthy observations is much higher for the first damage, being above 50%, whereas the healthy observations make up about 10% of the total observations for the second damage. Generally, the classification performance using the full frequency range of 100 - 3,000 Hz and the trimmed frequency range of 600 - 2,500 Hz is more similar for the second damage than for the first damage. Still, discarding the lower and higher end of the frequency range yields better performance for the second damage. Overall, compared to the first damage, a higher number of PCs is necessary to obtain near-perfect classification accuracy for the second damage.

Generally, using PCs corresponding to 95% of the variance explained yields high classification accuracy. Thus, this value is selected for dimensionality reduction. The resulting number of PCs, which are to be used for outlier analysis, are listed for all accelerometer channels in Table 3. One general observation that can be made is that the sensor channels placed on the shear web closest to the vibration shaker, e.g. channels 1, 9, 11, and 12, have a lower number of PCs explaining 95% of the variance, compared to the accelerometer channels placed away from the shear web, similar to what was observed for the first damage.

Table 3. Number of PCs required to explain 95% of the variance of the original data for all accelerometer channels, used as features for outlier detection.

Accelerometer channel number	Number of PCs explaining 95% of the variance
1	7
2	38
3	31
4	34
6	23
7	35
8	28
9	8
10	23
11	13
12	11

Detection of initiation and progression of damage: For outlier analysis, the same approach as for the previous damage is taken: The Mahalanobis distance is used as a damage index, and a threshold for the healthy state is calculated with a 99% confidence interval based on every second observation from the first 90% of the healthy data, such that more variability of the data is incorporated. The damage index D is plotted for all observations and accelerometer channels in Figure 20. Generally, the classification accuracy for the healthy data is within the confidence interval, and all damaged observations are classified as outliers. A clear jump in the damage index can be observed for most of the accelerometer channels starting after the introduction of the second damage at its initial length of 30 mm. A clear jump in the damage index for the subsequent manual increases in damage length is however not visible for most of the accelerometer channels. The manual increase to 400 mm damage length causes a jump in the damage index for channels 1, 2, 4, 6, 7, 10, and 11, while this significant increase in the damage length is not clearly visible from the damage index of the remaining channels.

The last vertical dotted line in the damage index plots marks the point in time at which the second damage propagated through the remainder of the shear web laminate, as shown in Figure 4(a-c), which causes a clear jump in the damage index for e.g. channel 9. Shortly following this vertical dotted line, another jump in the damage index is visible for e.g. channels 7 and 12, which is deemed to be due to further sudden cracking of the shear web laminate. Following this point, the damage index increases monotonically for e.g. channel 10 in line with further damage propagation towards the spar cap.

For some of the channels, e.g. channels 4 and 7, another large change in the damage index occurs towards the end of testing with this damage. Over a short span in the number of observations, the damage index is observed to drop with a magnitude close to that of the previously mentioned event where the web laminate cracked. It is not clear what event caused this change in the damage index, but it may be due to further damage propagation into the spar cap laminate.

Conclusions and discussions

This work investigated a wind turbine blade structural health monitoring campaign, focusing on detection and monitoring of two shear web cracks in a 52-meter wind turbine blade. Modal parameters of the lower-order natural vibration modes were found to show no significant changes as a result of the induced damages. Towards detection of small damages in large wind turbine blades, an active vibration monitoring system was designed. The monitoring system used an electrodynamic vibration shaker to excite the blade at frequencies between 100 and 3,000 Hz, and the vibration response was measured with accelerometers. Based on the PSD from the accelerometer outputs, changes coinciding with damage introduction and in line with damage progression were used to detect and monitor damage in the wind turbine blade.

Both shear web cracks investigated in this work could be detected through use of the active vibration monitoring system, showing significant increases in damage index following the artificial introductions of the damages. One of the main differences between the two damages was their location relative to the vibration shaker and accelerometers. The second damage was located in the path between the vibration shaker and the accelerometers, while the first damage was not. Both damages could be detected, showing that a damage does not need to be located in the path between the active vibration input and accelerometers. Thus, it is deemed that damage detection, in this case, is enabled through damages changing the local vibration response of the blade, which can be detected by accelerometers.

Based on the presented data, it has been shown that detection of damage initiation and progression is feasible using an actuator and a single vibration sensor placed within 10 meters of the location of a damage. It would be interesting to extend the present study to distributing accelerometers over the entire length of a wind turbine blade, and possibly using a more powerful vibration shaker, such that the effective damage detection range can be determined.

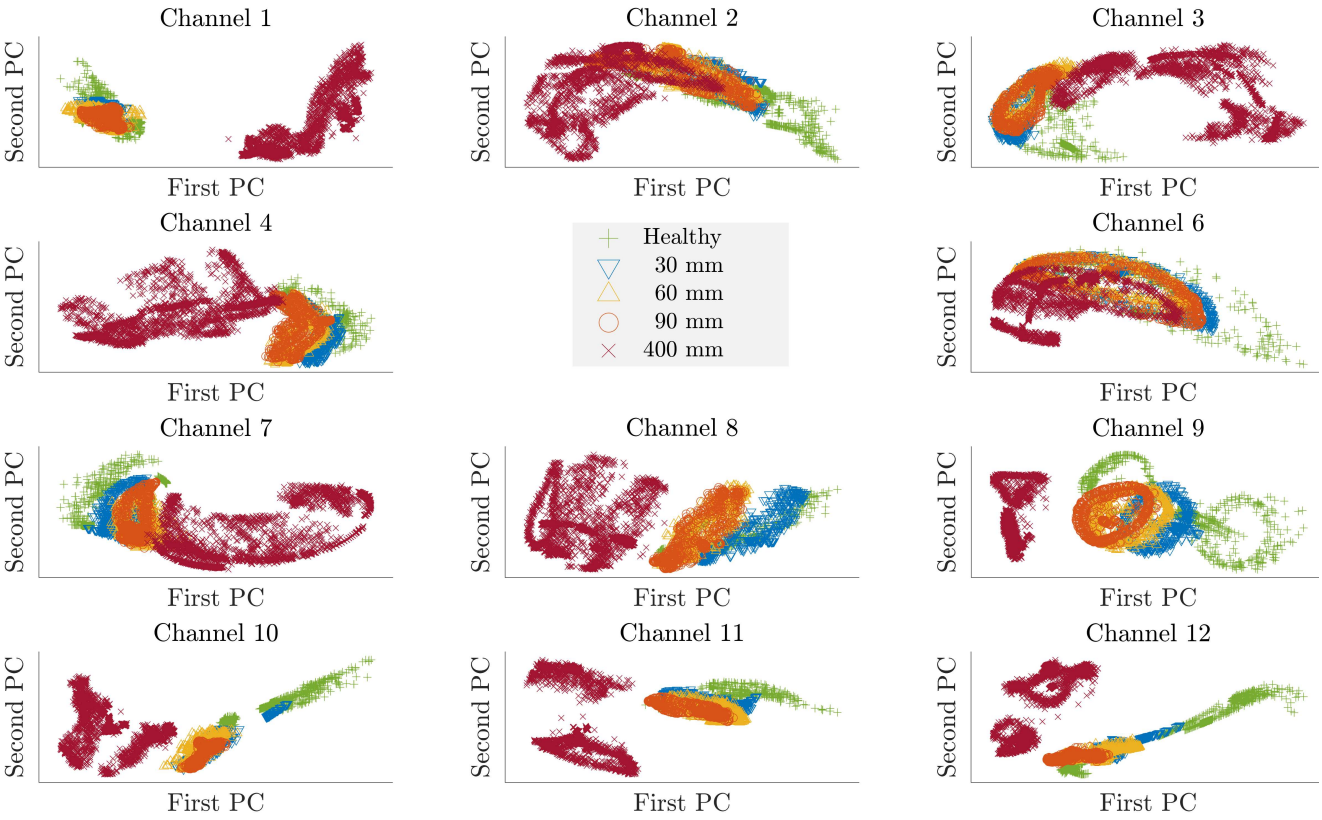

Figure 18. First two PCs for the PSD data from all accelerometers, using frequencies between 600 and 2,500 Hz.

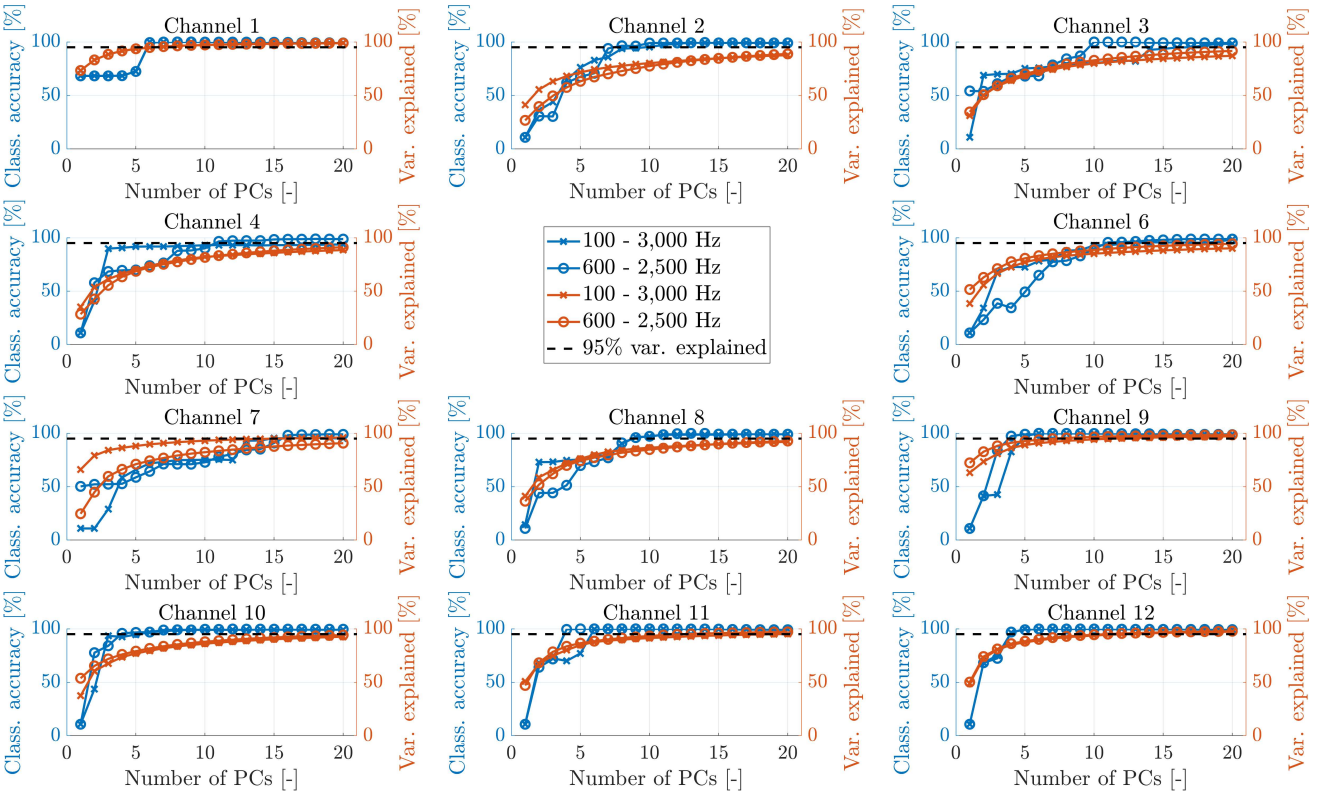

Figure 19. Classification accuracy (Class. accuracy) and variance explained (Var. explained) as a function of the number of PCs, plotted for all accelerometer channels, both using the full frequency range of 100 - 3,000 Hz as well as the trimmed frequency range of 600 - 2,500 Hz. It should be noted that the lower limit of the second axis depicting classification accuracy is set to 0% for all accelerometer channels, which differs from the corresponding plot shown for the first shear web damage, see Figure 15.

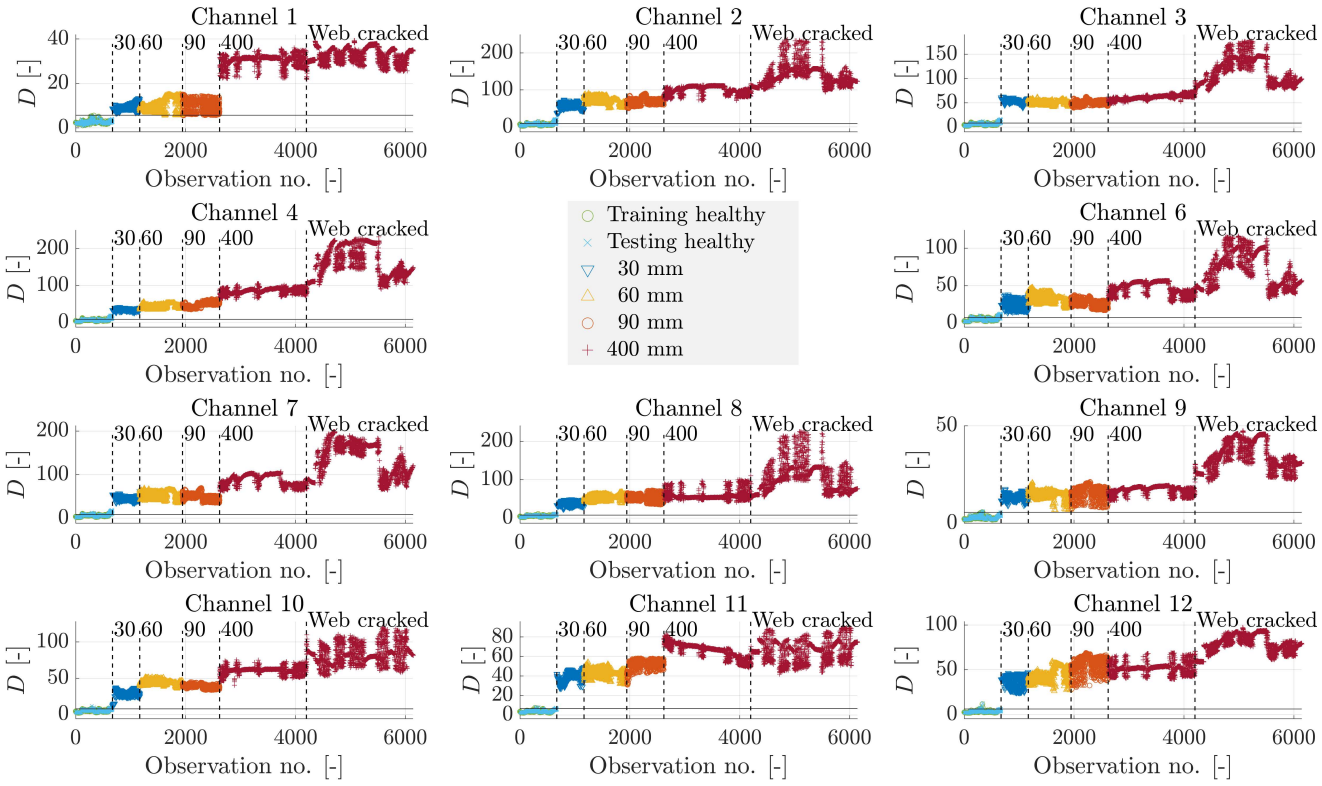

Figure 20. Plot of damage index D, calculated based on the Mahalanobis distance by using PCs explaining 95% of the variance of the original data. The horizontal solid line marks the 99% confidence threshold, allowing for 1% false positives in the training data. The vertical dotted lines mark the manual introduction and manual increase in length of the second damage, including a significant event in fatigue-driven damage propagation (web cracked).

Ultimately, the range required of a monitoring system depends on whether the desired function is monitoring of a specific part of a wind turbine blade or monitoring of an entire wind turbine blade.

Regarding sensor placement, the locations of the accelerometers used for the present study were selected based on engineering judgment. Locations on the shear web were used due to the signal-to-noise ratio of the output from the active vibrations being expected to be sufficiently high to ensure detection of changes in the vibration response of the web laminate caused by initiation and propagation of the damages. Locations on the spar cap and shell laminate were used as well to investigate if detection of damages in the web would be possible using sensors located on other parts of the blade laminate, where the signal-to-noise ratio would be lower. As discussed previously, the sensor placement is believed to be of great importance, since sensors need to be placed at locations that are sensitive to vibration modes impacted by the presence of the damage that is desired to be detected. If a damage of a specific type or with a specific location is of interest, it may be relevant to perform studies on optimal sensor placement. In this way, the number of sensors required for detection of specific damages can be minimized, which in turn will make the sensing system less costly and make it more economically feasible for real-life applications.

Dimensionality reduction of the PSDs was performed with PCA, and it was found that the healthy and damaged states were well-separated for some of the measurement channels at low dimensionality, whereas higher dimensionality was required for some measurement channels. Still, using a general criterion of PCs explaining 95% of the variance yielded good performance in outlier detection for all accelerometer channels. Investigating the number of PCs required to obtain high classification accuracy, it was found that a naive choice of the number of PCs based on e.g. 95% of the variance explained was not the optimal choice. Adding PCs after a certain number, where near-perfect classification accuracy was obtained, resulted in more noise being included in the feature space. Moreover, following successful separation between healthy and damaged observations, an increased number of PCs may be required to separate multiple damaged states and infer damage progression. Consequently, inference of damage propagation may be increasingly difficult with accelerometers being placed further from the active vibration input. Another observation that was made was that using too few PCs would result in observations from the damaged state sampled during stand-still of the fatigue test being wrongly classified as inliers. Thus, correct classification of observations from both operational states requires a certain number of PCs. It may be of interest to perform studies on optimal number of PC selection, which should ideally result in the formulation of general recommendations that are also useful for real-life applications, where data for the damaged state of a structure is not available.

Based on the frequency range ultimately used for feature extraction, which has been shown to contain damage-sensitive features, the input frequencies applied by the vibration shaker could be reduced from 100 - 3,000 Hz

to 600 - 2,500 Hz for the case of damage detection in a blade during fatigue testing. Consequently, the length of the input signal can be decreased significantly, allowing for an increased number of observations to be sampled within a given time, as well as reducing the amount of data for each observation. For the case of monitoring a blade on an operating turbine, the effective frequency range for damage detection may be different than what was found in the present study, but this can be determined by comparing the noise level from the presented fatigue test to the noise level from an operating turbine. Additionally, the coherence may be used to investigate which frequencies are excited well at different sensor locations. This information may be used to further narrow down the frequency range useful for detection and monitoring of damages.

The present work has in some sense investigated the use of higher-order vibration modes, through the PSDs, in use as features for detection of damage. As an extension to this, the higher-order mode shapes, associated with local vibration modes, could also be investigated for use in damage detection. To facilitate this, a denser sensor network than the one used in the present work would be required.

This work investigated detection and monitoring of laminate cracks, which were believed to alter the local stiffness and as such the local vibration response of the blade laminate, which in turn could be measured through the frequency response at different locations on the blade laminate. Considering the case of e.g. delaminations, the local stiffness would be impacted to a lessened degree, as long as no local buckling occurs. As such, the robustness of the proposed method for detection of other failure modes may be of interest for investigation in future work.

Since the blade test campaign was performed in a temperature-controlled environment, it does not accurately include the environmental and operational conditions of blades in operating wind turbines. Nevertheless, it is argued that data was investigated for two different operational states of the blade: stand-still, with little external noise; and fatigue testing, where significant noise was present due to the rotating mass fatigue exciter. Data from both these operational states was included in the covariance of the healthy state as well as for training of a threshold for outlier analysis, which resulted in all damaged observations being classified as outliers in both of the investigated operational states. Even though environmental and operational conditions will differ for blades in operating turbines, it is believed that the proposed method will be applicable in such conditions, as long as they are accounted for in the training data. Alternatively, environmental and operational effects can be accounted for through additional signal processing steps, which has been outside the scope of the present work. Additionally, the rotational speed of the rotor will add harmonics to the frequency response extracted from accelerometer measurements. Compared to the investigated frequency range, the rotational speed is much lower, but this effect should still be kept in mind, and its possible influence on the results obtained through the used signal processing methods should be accounted for.

The purpose of SHM systems is to enable automated monitoring of structures. For operating turbines, a threshold for the healthy state needs to be set based on measurements collected during commissioning and over a period following the installation of the turbine. A threshold for the healthy state needs to be set for each blade in a turbine, since there will be variations from turbine to turbine as well as from blade to blade, which will affect any measurements collected. Moreover, tolerances on sensor location, sensor adhesion, sensor sensitivity, etc. will cause variations in measurements, which have to be accounted for by individualizing thresholds for the healthy state of each blade.

A limitation found in the presented results is the sensitivity of the method for separation of the damage lengths between 30 and 90 mm for the second investigated shear web damage, i.e. detection of very gradual damage propagation. Towards this, the use of other signal processing methods for feature extraction and outlier methods may provide higher sensitivity, which should be investigated.

Another investigation which is relevant towards the practical implementation of the proposed active vibration monitoring system for blades on operating turbines is the long-term effect of the active vibration input on the blade laminate. The force applied by the vibration shaker is very low compared to the forces acting on wind turbine blades. Nevertheless, it should be ensured that the use of an active vibration monitoring system does not in itself result in degradation of the blade laminate.

Concerning planning of inspections and repairs, using any observations that barely exceed the healthy threshold is most likely an overly conservative approach. As such, for the present SHM system, a threshold value for the damage index needs to be set, at which a potential damage is deemed to have reached a size critical enough to warrant manual inspection and/or repair of the damage. This threshold value would be higher than the threshold value set for defining the healthy state of the blade since the presence of small, non-critical damages can be accepted. Based on the observations in the damage indices in the present study, it is challenging to set a single value as a threshold for repair or inspection. The damage indices varied in magnitude across the accelerometer channels, adding to the uncertainty of defining a single magnitude for a threshold to be used as a trigger for scheduling inspection or repair. Furthermore, different types of damages with different locations may result in different magnitudes of damage indices, making it further difficult to establish a single magnitude for inspection or repair. Alternatively, it may be sensible to define a criterion based on changes in damage indices occurring over time. As observed in this work, the damage index for some accelerometer channels exhibited a decrease with increasing damage severity, which would not be detectable if a static threshold value were to be set for triggering alarms.

Towards the practical implementation of SHM systems, a business case needs to be established, which accounts for the cost of periodic manual inspection and risk of blade failure versus the costs of investing in a blade SHM system. With increased digitalization, the authors believe that blades will, in the near future, be sensor-equipped, e.g. through embedded sensing technology. Application of an active input is believed to be possible through e.g., pitching of blades or through active flaps. Thus, employing an active vibration monitoring system for wind turbine blades is believed to become a profitable business case.

Further work is ongoing regarding comparison of different signal processing methods and their performance in severity assessment of damage.

Acknowledgements

This work received partial funding from the Innovation Fund Denmark, grant no. 9065-00200B. This work is partly supported by the Danish Energy Agency through the Energy Technology Development and Demonstration Program (EUDP), grant no. 64018-0068. The supported project is RELIABLADE: Improving Blade Reliability through Application of Digital Twins over Entire Life Cycle.

References

1. Christine Röckmann SL and Stavenuiter J. Operation and Maintenance Costs of Offshore Wind Farms and Potential Multi-use Platforms in the Dutch North Sea. In *Aquaculture Perspective of Multi-Use Sites in the Open Ocean*, chapter 4. Springer. ISBN 9783319511597, 2017. pp. 97–113. DOI: 10.1007/978-3-319-51159-7.
2. Dao C, Kazemtabrizi B and Crabtree C. Wind turbine reliability data review and impacts on levelised cost of energy. *Wind Energy* 2019; 22(12): 1848–1871. DOI:10.1002/we.2404.
3. McGugan M, Pereira G, Sorensen BF et al. Damage tolerance and structural monitoring for wind turbine blades. *Philosophical Transactions of the Royal Society A: Mathematical, Physical and Engineering Sciences* 2015; 373(20140077). DOI: 10.1098/rsta.2014.0077.
4. Martinez-Luengo M, Kolios A and Wang L. Structural health monitoring of offshore wind turbines: A review through the Statistical Pattern Recognition Paradigm. *Renewable and Sustainable Energy Reviews* 2016; 64: 91–105. DOI:10.1016/j.rser.2016.05.085. URL http://dx.doi.org/10.1016/j.rser.2016.05.085.
5. Civera M and Surace C. Non-Destructive Techniques for the Condition and Structural Health Monitoring of Wind Turbines: A Literature Review of the Last 20 Years. *Sensors* 2022; 22(4). DOI:10.3390/s22041627.
6. Structural health monitoring – do you need to test the integrity of a structure over time?, 2022. URL https://svibs.com/applications/structural-health-monitoring/.
7. Lorenzo ED, Manzato S, Peeters B et al. Modal Analysis of Wind Turbine Blades with Different Test Setup Configurations. In *Topics in Modal Analysis & Testing*, volume 8. ISBN 9783030126834, 2019. pp. 143–152.
8. Lorenzo E, Manzato S, Luczak M et al. Strain-based operational modal analysis for wind turbine blades. In *Proceedings of the 8th International Operational Modal Analysis Conference IOMAC*. p. 012022.
9. Luczak MM, Peeters B, Manzato S et al. Research sized wind turbine blade modal tests : comparison of the impact excitation with shaker excitation. In *J. Phys.: Conf. Ser. 1102*. p. 012022.
10. Lorenzo ED, Petrone G, Manzato S et al. Damage detection in wind turbine blades by using operational modal analysis. *Structural Health Monitoring* 2016; 15(3): 289–301.
11. Larsen G, Berring P, Tcherniak D et al. Effect of a damage to modal parameters of a wind turbine. In *Proceedings of the 7th European Workshop on Structural Health Monitoring*. p. 9.
12. Ulriksen MD, Tcherniak D, Kirkegaard PH et al. Operational modal analysis and wavelet transformation for damage identification in wind turbine blades. *Structural Health Monitoring* 2015; 15(4): 381–388. DOI:10.1177/1475921715586623.
13. Al-Khudairi O, Hadavinia H, Little C et al. Full-scale fatigue testing of a wind turbine blade in flapwise direction and examining the effect of crack propagation on the blade performance. *Materials* 2017; 10(10). DOI:10.3390/ma10101152.
14. Fremmelev MA, Ladpli P, Orlowitz E et al. Structural health monitoring of 52-meter wind turbine blade: Detection of damage propagation during fatigue testing. *Data-Centric Engineering* 2022; DOI:10.1017/dce.2022.20.
15. Chen X, Semenov S, McGugan M et al. Fatigue testing of a 14.3 m composite blade embedded with artificial defects – Damage growth and structural health monitoring. *Composites Part A: Applied Science and Manufacturing* 2021; 140(November 2020): 106189. DOI:10.1016/j.compositesa.2020.106189. URL https://doi.org/10.1016/j.compositesa.2020.106189.
16. Tan L, Saito O, Yu F et al. Impact Damage Detection Using Chirp Ultrasonic Guided Waves for Development of Health Monitoring System for CFRP Mobility Structures. *Sensors* 2022; 22(3). DOI:10.3390/s22030789.
17. Ruan J, Ho SCM, Patil D et al. Structural health monitoring of wind turbine blade using piezoceremic based active sensing and impedance sensing. *Proceedings of the 11th IEEE International Conference on Networking, Sensing and Control, ICNSC 2014* 2014; : 661–666DOI:10.1109/ICNSC.2014.6819704.
18. Taylor SG, Jeong H, Jang JK et al. Full-scale fatigue tests of CX-100 wind turbine blades. Part I: testing. *Industrial and Commercial Applications of Smart Structures Technologies 2012* 2012; 8343(March 2012): 83430Q. DOI:10.1117/12.917497.
19. Taylor SG, Jeong H, Jang JK et al. Full-scale fatigue tests of CX-100 wind turbine blades. Part II: analysis. *Industrial and Commercial Applications of Smart Structures Technologies 2012* 2012; 8343(March 2012): 83430Q. DOI:10.1117/12.917497.
20. Dervilis N, Choi M, Antoniadou I et al. Novelty detection applied to vibration data from a CX-100 wind turbine blade under fatigue loading. *Journal of Physics: Conference Series* 2012; 382: 1–6. DOI:10.1088/1742-6596/382/1/012047.
21. Dervilis N, Choi M, Taylor SG et al. On damage diagnosis for a wind turbine blade using pattern recognition. *Journal of Sound and Vibration* 2014; 333(6): 1833–1850. DOI:10.1016/j.jsv.2013.11.015. URL http://dx.doi.org/10.1016/j.jsv.2013.11.015.
22. Dervilis N, Choi M, Antoniadou I et al. Machine learning applications for a wind turbine blade under continuous fatigue loading. *Key Engineering Materials* 2014; 588(October): 166–174. DOI:10.4028/www.scientific.net/KEM.588.166.
23. Yang W, Lang Z and Tian W. Condition Monitoring and Damage Location of Wind Turbine Blades by Frequency Response Transmissibility Analysis. *IEEE Transactions on Industrial Electronics* 2015; 62(10): 6558–6564. DOI:10.1109/TIE.2015.2418738.
24. Schulz MJ and Sundaresan MJ. Smart Sensor System for Structural Condition Monitoring of Wind Turbines Smart Sensor System for Structural Condition Monitoring of Wind

Turbines. *North* 2006; .

25. Ghoshal A, Sundaresan MJ, Schulz MJ et al. Structural health monitoring techniques for wind turbine blades. *Journal of Wind Engineering and Industrial Aerodynamics* 2000; 85(3): 309–324. DOI:10.1016/S0167-6105(99)00132-4.
26. Tcherniak D and Mølgaard LL. Vibration-based SHM system: Application to wind turbine blades. *Journal of Physics: Conference Series* 2015; 628(1). DOI:10.1088/1742-6596/628/1/012072.
27. Ulriksen MD, Tcherniak D and Damkilde L. Damage detection in an operating Vestas V27 wind turbine blade by use of outlier analysis. In *2015 IEEE Workshop on Environmental, Energy, and Structural Monitoring Systems, EESMS 2015 - Proceedings*. Institute of Electrical and Electronics Engineers Inc. ISBN 9781479982141, pp. 50–55. DOI:10.1109/EESMS.2015.7175851.
28. Tcherniak D and Mølgaard LL. Active vibration-based structural health monitoring system for wind turbine blade: Demonstration on an operating Vestas V27 wind turbine. *Structural Health Monitoring* 2017; 16(5): 536–550. DOI:10.1177/1475921717722725.
29. García D and Tcherniak D. An experimental study on the data-driven structural health monitoring of large wind turbine blades using a single accelerometer and actuator. *Mechanical Systems and Signal Processing* 2019; 127: 102–119. DOI:10.1016/j.ymssp.2019.02.062.
30. Panagiotopoulos A, Tcherniak D and Spilios FD. Damage detection on the blade of an operating wind turbine via a single vibration sensor and statistical time series methods: Exploring the performance limits of robust methods. *Structural Health Monitoring* 2022; 0(0). DOI:10.1177/14759217221094493.
31. Van Overschee P and De Moor B. *Subspace Identification for Linear Systems*. Kluwer Academic Publishers Group, 1996. ISBN 9781461304654. DOI:10.1007/978-1-4613-0465-4.
32. Brandt A. ABRAVIBE – A MATLAB toolbox for noise and vibration analysis and teaching, 2011. http://www.abravibe.com.
33. Orlowitz E. *Damping Estimation in Operational Modal Analysis*. PhD Thesis, University of Southern Denmark, 2015.
34. Worden K, Sohn H and Farrar CR. Novelty detection in a changing environment: Regression and interpolation approaches. *Journal of Sound and Vibration* 2002; 258(4): 741–761. DOI:10.1006/jsvi.2002.5148.
35. Farrar CR and Worden K. *Structural Health Monitoring: A Machine Learning Perspective*. John Wiley and Sons Ltd, 2012. ISBN 9781119994336. DOI:10.1002/9781118443118.
36. Stoica, Petre and Moses, Randolph. *Spectral Analysis of Signals*. New Jersey 07458: Prentice Hall, 2004. ISBN 0131139568.
37. Bishop CM. *Pattern Recognition and Machine Learning*. Springer, 2006. ISBN 9780387310732. DOI:10.1007/978-3-030-57077-4_11.
38. Stewart GW. On the early history of the singular value decomposition, 1992.